Study On Different Metal Oxide with *Hylocereus polyrhizus* (Dragon Fruit) in Dye-Sensitized Solar Cells Performance

HARTATI BINTI KATU MAHMUD

F15A0049

A thesis submitted in fulfillment of the requirements for the degree of Bachelor of Applied Science (Bioindustrial Technology) with Honors

FACULTY OF BIOENGINEERING AND TECHNOLOGY
UNIVERSITI MALAYSIA KELANTAN

2019

DECLARATION

I hereby declare that the work embodied in this report is the results of the original research and has not been submitted for a higher degree to any universities or institutions.

_____

Student

Name: Hartati Binti Katu Mahmud

Date:

I certify that the report of this final year project entitled "Study on Different Metal Oxide with Hylocereus polyrhizus sp. (Dragon Fruit) in Dye-Sensitized Solar Cells Performance" by Hartati Binti Katu Mahmud, F15A0049 has been examined and all the correction recommended by examiners have been done for the degree of Bachelor of Applied Science (Bioindustrial Technology) with Honours, Faculty of Bioengineering and Technology, Universiti Malaysia Kelantan.

Approved by:

_____

Supervisor

Name: Dr. Hasyiya Karimah Binti Adli

Stamp:

Date:

ACKNOWLEDGEMENT

In the name of Allah, the Most Gracious and the Most Merciful

Alhamdulillah, all praises to Allah for the strength and His blessing for me to complete this research.

First and foremost, I would like to say thank you to the Universiti Malaysia Kelantan for giving me the chance and experience to carry out the Final Year Project. Next, I would like to express my very special thanks and gratitude to my supervisor, Dr. Hasyiya Karimah Binti Adli for giving me the opportunity to join the group, guiding and encouraging me. Without her guidance and support, it would be difficult in completion this research study. It was a great and fantastic experience to work with you.

Besides, I would like to give very special thanks to Dr. Syed Muhammad Al-Amsyar for his cooperation and suggestions in this project. Besides, my sincere appreciation also goes to Pn. Hasiah from UMT, all lecturers, laboratory assistants and UMK staffs in helping me in many different ways to complete this research.

I also acknowledge my gratitude to my parents for their sacrifice, support and patience to ensure that I would manage to complete this research study in ease. Beside, I would like to say thank you to my final year project group, Ashma, Chien, Fahmi and Soon Wei for aiding me multiple times during the research. Lastly, my appreciation and thanks to those whom contributed in this project directly which I believe, without their suggestions and comments for this research could be impossible to complete.

Thank you so much.

TABLE OF CONTENTS

LIST OF TABLES

LIST OF FIGURES

LIST OF ABBREVIATIONS AND SYMBOLS

TW	Terawatts
CO_2	Carbon dioxide
PV	Photovoltics
DSSC	Dye-sensitized solar sells
TiO_2	Titanium oxide
Al_2O_3	Aluminium oxide
ZnO	Zinc oxide
1G	First generation
2G	Second generation
3G	Third generation
4G	Fourth generation
PEC	Photoelectrochemical
PSCs	Polymer solar cells
nm	Nanometer
$COOH^-$	Carboxylic acid
$H_2PO_3^-$	Phosphorous acid
SO_3H^-	Sulfonic acid
Al	Aluminium
HOMO	Highest occupied molecular orbital
LUMO	Lowest unoccupied molecular orbital
ITO	Indium tin oxide
UV-Vis	Ultraviolet-visible spectrophotometer
SEM	Scanning electron microscopy

4PP	Four point probe
EIS	Electrochemical impedance spectra
DF	Dragon fruit
cm	Centimeter
g	Gram
kg	Kilogram
mL	Mililiter
µm	Micrometer
°C	Degree celcius
AO	Aluminium oxide
ZO	Zinc oxide
TO	Titanium oxide
Voc	Open-circuit voltage
Isc	Short-circuit photocurrent
FF	Fill factor
V	Voltage
nm	Nanometer
UV	Ultraviolet
λ	Wavelength
h	Planck's constant
c	Speed of light
Rs	Sheet resistance
σ	Conductivity
IV	Current –Voltage
PCE	Power conversion efficiency

Study On Different Metal Oxide With *Hylocereus polyrhizus* (Dragon Fruit) in Dye-Sensitized Solar Cells Performance

ABSTRACT

The energy crisis becomes a serious issue for every country in the world. The world's demand depends on the inadequate energy from resources such as oil and fossil fuel that are diminishing due to nonstop consumption. Thus, few renewable energy as unconventional energy have been explored, including solar energy. A solar cell use the energy of the sun and transforms it into electricity. Dye-sensitized solar cell (DSSC) transforms visible light energy through separation in photo-absorber layer of a wide gap semiconductor. Dye-sensitized solar cells have several layers including light absorber dye and an active electrode, in which in this study three different metal oxides of photoanode which are titanium dioxide, TiO_2 (**TO**) nanoparticles, zinc oxide, ZnO (**ZO**) and aluminum oxide, Al_2O_3 (**AO**) were prepared and examined each performance in DSSC. The extraction of *Hylocereus polyrhizus* (dragon fruit) coated on three different metal oxides were characterized with several analysis such as UV–Vis absorption spectroscopy, scanning electron microscopy (SEM), four point probe (4PP) and electrochemical impedance spectra (EIS). It was found that *Hylocereus polyrhizus* extract has good absorbance and the bandgap value recorded was 2.15 eV. With dye extract coated on metal oxides (**MO**), the **TO**/**DF**/ITO has the lowest bandgap value which is 1.55 eV, compared to **ZO**/**DF**/ITO and **AO**/**DF**/ITO with value of 2.60 and 2.80 eV respectively. Besides, the surface morphology viewed by SEM analysis exhibited morphology of each **MO**/**DF**/ITO has different in particles sizes and surface. Results from 4PP, shows the sheet resistance values of **DF**/ITO, **TO**/**DF**/ITO, **AO**/**DF**/ITO and **ZO**/**DF**/ITO are 26.69, 13.78, 23.39 and 18.58 Ωm respectively. The conductivity values of **DF**/ITO, **TO**/**DF**/ITO, **AO**/**DF**/ITO and **ZO**/**DF**/ITO are 3.75E-04, 7.26E-04, 4.28E-04 and 5.38E-04 Scm^{-1}, respectively while power conversion efficiency (PCE) **TO**/**DF**/ITO performed the highest with 5.20 % followed with **ZO**/**DF**/ITO, **AO**/**DF**/ITO and **DF**/ITO with 4.35 %, 3.32 % and 1.58 %, respectively.

Keywords: photo-absorber, electronic bandgap, titanium dioxide nanoparticles, aluminium oxide, zinc oxide.

Mengkaji Logam Oksida Yang Berbeza Dengan *Hylocereus polyrhizus* (Dragon Fruit) Dalam Prestasi Sel Suria Terpeka Pewarna

ABSTRAK

Krisis tenaga merupakan masalah yang serius pada seriap negara di dunia. Permintaan dunia bergantung pada sumber tenaga yang terhad seperti minyak dan bahan bakar fosil yang berkurang akibat daripada penggunaan tanpa henti.Oleh yang demikian, beberapa tenaga boleh diperbaharui sebagai tenaga bukan konvensional telah diterokai, termasuk tenaga solar. Sel solar menggunakan tenaga matahari dan menukarkan menjadi tenaga elektrik. Sel suria terpeka pewarna (DSSC) menukarkan tenaga cahaya nampak melalui pemisahan di dalam lapisan penyerap-cahaya oleh semikonduktor lurang lebar. Sel suria terpeka pewarna mempunyai beberapa lapisan termasuk penyerap cahaya dan elektrod yang aktif, dimana dalam pembelajaran ini tiga logam oksida yang berbeza fotoanod iaitu titanium dioksida, TiO_2 (**TO**) nanopartikel, zink oksida, ZnO (**ZO**) dan aluminium oksida, Al_2O_3 (**AO**) telah dihasilkan dan dikaji setiap prestasi dalam DSSC. Ekstrak pewarna daripada *Hylocereus polyrhizus* (buah naga) disalut pada tiga logam oksida yang berbeza telah dianalisa menggunakan beberapa analysis seperti spektroskopi penyerapan UV-Vis, mikroskop elecktron pengimbasan (SEM), (4PP) dan (EIS). Telah didpati ekstrak *Hylocereus polyrhizus* mempunyai penyerapan yang baik dan luang jalur iaitu 2.15 eV. Dengan exstrak pewarna salut dengan logam okside (**MO**), **TO**/**DF**/ITO mempunyai lurang jalur yang lebih rendah iaitu 1.55 eV dibandingkan dengan nilai **ZO**/**DF**/ITO dan **AO**/**DF**/ITO iaitu dan 2.60 dan 2.80 eV. Selain itu, permukaan morfologi melalui analisis SEM yang telah dilihat telah menunjukkan perubahan morfologi dengan perbezaan saiz partikel dan permukaan. Keputusan yang diperolehi daripada 4PP, menunjukkan nilai rintangan kepingan **DF**/ITO, **TO**/**DF**/ITO, **AO**/**DF**/ITO dan **ZO**/**DF**/ITO iaitu 26.69, 13.78, 23.39 dan 18.58 Ωm. Di samping itu, nilai kekonduksian untuk **DF**/ITO, **TO**/**DF**/ITO, **AO**/**DF**/ITO dan **ZO**/**DF**/ITO ialah 3.75E-04, 7.26E-04, 4.28E-04 Scm^{-1} dan 5.38E-04 Scm^{-1}. Kecekapan penukaran kuasa (PCE) menunjukkan **TO**/**DF**/ITO adalah yang tertinggi dengan 5.20 % diikuti oleh **ZO**/**DF**/ITO, **AO**/**DF**/ITO dan **DF**/ITO iaitu 4.35 %, 3.32 % dan 1.58 %.

Kata kunci: penyerap-cahaya, luang jalur, titanium oksida nanopartikel, aluminium oksida, zink oksida.

CHAPTER 1

INTRODUCTION

1.1 Background of Study

Recently, there has been an increasing concern regarding on global energy crisis. Many researchers had acknowledged about the mismatch between the energy supply and energy demands which are become critical and biggest issues that we are facing today. With constant growing of population of human and rapidly improved of living style, higher energy recourses are needed. Currently, it is estimated that the energy consumption for billions of people in the worldwide is about 14 terawatts (TW) and it is expected to increase to another 10 TW in the next 40 years (Gräetzel, 2009).

In 2014, the worldwide energy consumption primarily originates from fossil fuels come from oil (35.7 %), coal (19.3 %), gas (25.0 %) and renewable energy sources (9.5 %), which illustrated in Figure 1.1. This leads to the significant of environmental concerns such as high levels of carbon dioxide (CO_2) emissions (Goncalves *et al*., 2008). With continues

usage of fossil fuels in industry, the amount of greenhouse gasses emission is expected continues to rise.

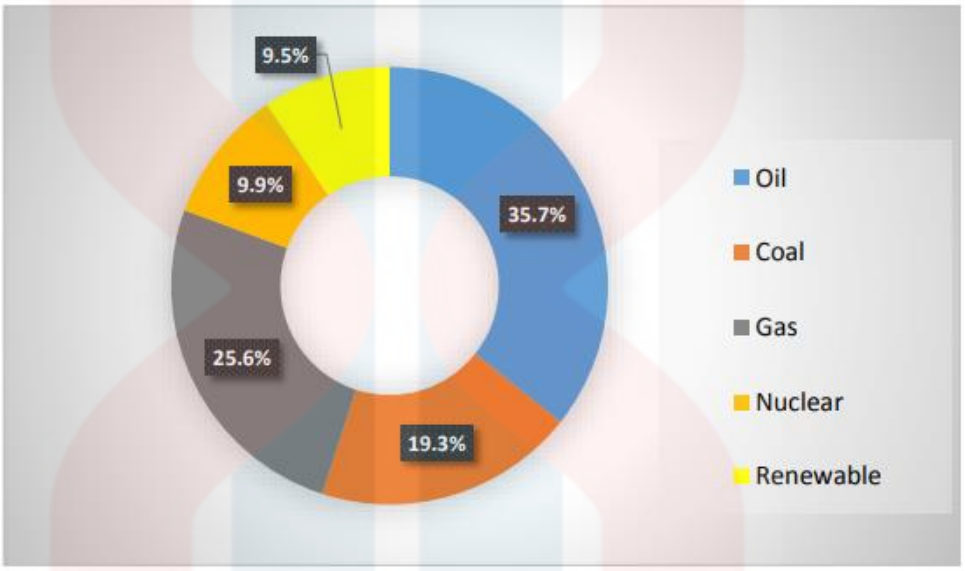

Figure 1.1: Global energy consumption (World Energy Outlook, 2014)

The most problematic issues facing nowadays is about the depletion of fossil fuel associated with the continually increasing demand. The energy from fossil fuels causes major problems, which are limited of resources and is the environmental impact. Because of these major problems, an increased of global awareness makes the urgent need of researcher to come out with an alternative of other energy resources.

Therefore, the supply of sustainable energy is considered to become one of the most important technical challenges and scientific facing humanity in the 21st century (Nocera & Nash, 2007). These undesirable problems has led to the presence of the growth of renewable energy such as hydroelectric power, geothermal energy, biomass, wind power

and solar power which importantly to overcome the dearth. Thus, solar energy is the best of renewable energy that would be sufficient to cover the 0.1 % of the earth's surface because it is suitable, safe and low-cost (Gräetzel, 2009).

Solar cells are also known as photovoltaics (PV), which are devices transforming the energy of the sunlight into electricity by the photovoltaic effect. Over the past century, the field of PV research has been developed significantly. PV effect occurs when photons are hitting upon semiconductor and producing an electron-hole pair. The electron and hole then be directed to two different connections, to finally form an electric potential difference. Einstein published his theory of the photoelectric effect, in which the possibility for individual photons could eject the electrons from atoms and putting them back at the higher levels of energy state (Klassen, 2011).

The Einstein's theory of the light quanta had been confirmed by Arthur Compton's experiments and theoretical explanation (Klassen, 2011). Initially, the power conversion efficiency (PCE) was very low that scientists were not very interested until Bell lab announced 6 % of PCE from silicon solar cell. Since then silicon crystalline solar cells have been dominated the solar manufacturing with the highest cell efficiency (25 %), with other type of solar cells, as shown in Figure 1.2.

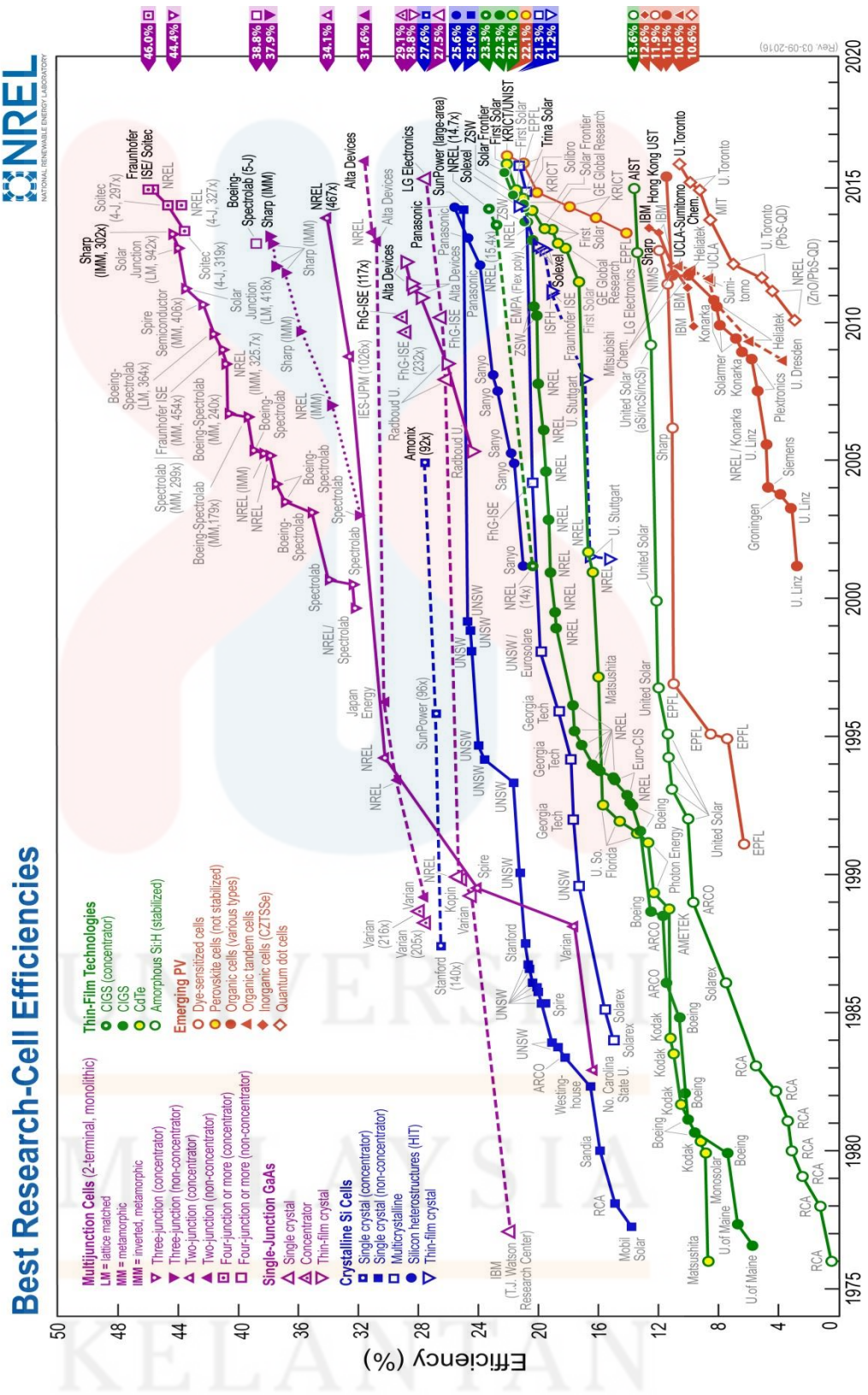

Figure 1.2**:** Recent percentage of photovoltaic cell development (NREL, 2016)

1.2 Problem Statement

The energy crisis is a worldwide issue as the world is now facing acute shortage of non-renewable resources such as petroleum, gold, coal and natural gas. Dramatic increase of consumption of these energy resources raised alarming signals to the existing resource base. Therefore, the renewable energy such as solar energy is one of the way out to overcome the energy crisis. The fabrication of dye-sensitized solar cells (DSSCs) based on natural dyes extracts become widely implemented due to the low-cost solar cell approach, environmental-friendly and easy fabrication.

Hence, in this study, the preparation of different metal oxides which are titanium oxide, TiO_2 (**TO**), zinc oxide, ZnO (**ZO**) and aluminium oxide, Al_2O_3 (**AO**), with dye extracts solution extracted from *Hylocereus polyrhizus sp*. (dragon fruit) flesh were carried out. The photo-absorber properties of resulted different metal oxide/dyes solution was expected to have different solar cell and conductivity properties performance. The outcomes of the study is the potential of metal oxides as photoanode and natural dye sensitizer (dragon fruit) in solar cell application. The selection of photoabsorber from natural resources can contribute to promising low-cost, environmentally, safe and comparable PCE.

1.3 Hypothesis

Titanium oxide, TiO_2 (**TO**) with *Hylocereus polyrhizus sp*. (dragon fruit) flesh dyes in dye-sensitized solar cell (DSSCs) would have highest conductivity compared to those with zinc oxide, ZnO (**ZO**) and aluminium oxide, Al_2O_3 (**AO**). This is can be expected due to its better in photo-absorption and physic and chemical properties.

1.4 Objectives

i. To extract *Hylocereus polyrhizus sp*. (dragon fruit, **DF**) as natural photo-absorber with the preparation of different metal oxides (**MO**) thin films from titanium oxide, TiO_2 (**TO**), zinc oxide, ZnO (**ZO**) and aluminium oxide, Al_2O_3 (**AO**).

ii. Fabrication of full completed dye-sensitized solar cells in the configuration of ITO/**MO**/DF/carbon, (**MO** are titanium oxide, zinc oxide and aluminum oxide).

iii. To carry out several physical analysis and conductivity properties using ultraviolet-visible spectrophotometer (UV-Vis), scanning electron microscopy (SEM), four point probe (4PP) and electrochemical impedance spectra (EIS).

1.5 Scope of Study

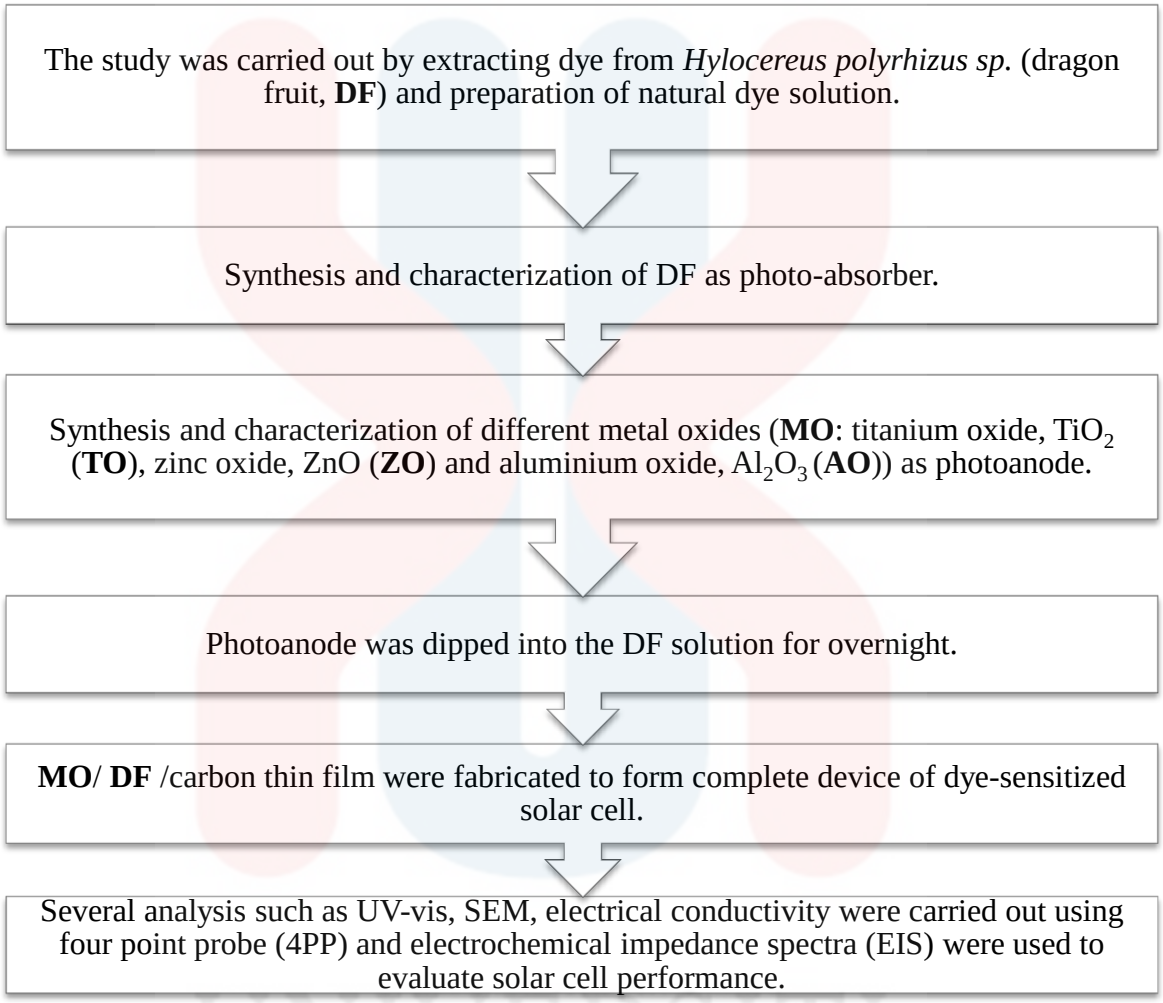

1.6 Significant of Study

The outcomes of the study is the potential of metal oxides as photoanode and natural dye sensitizer (dragon fruit) in solar cell application. The selection of photoabsorber from natural resources can contribute to promising low-cost, environmentally, safe and comparable PCE.

At the end of this study, the extraction of the natural dyes extracted from *Hylocereus polyrhizus sp.* (dragon fruits) and the approach of preparation of different metal oxide and dye extracts will be developed to evaluate its potential in dye-sensitized solar cell (DSSC). Thus, the exploration of these different metal oxide and dyes preparation will give promising approaches the conductivity properties for further development in DSSC.

CHAPTER 2

LITERATURE REVIEW

2.1 Energy Problem

The energy crisis is a serious issue facing by all countries in the world. Non-renewable energy resources such as fossil fuel and oil are in seriously depleted due to rapid consumption for industry and urbanization. The increase of the world's population combined with the growth per capita of energy consumption is expected to bring an explosive rise in energy consumption. Thus, to overcome the energy dependence on the non-renewable resources, other renewable energy have been explored including solar, wind, hydropower, geothermal and biomass energy. As for the renewable resources, it does not pollute the atmosphere and it is also capable to endure for long time. One of the best ideas is to make this happen is for solar cells application (Gräetzel, 2009).

2.2 Solar Energy

Generally, renewable energy is clean energy, cost-effective and efficient. In order to overcome the energy dependence on non-renewable resources, other renewable energy has been explored including solar, wind, hydropower, geothermal and biomass energy. Solar energy is suitable for the countries in the equatorial region with tropical rainforest climate, including Malaysia. The intensity of sunlight at the surface of the Earth is reported about one thousand watt per square meter (Shanmuga *et al*., 2016).

Based on the Figure 2.1, the solar energy can be classified into four generations, which the first generation of solar cell is well-known as to comprise of the photovoltaic technology based on the thick crystalline and inorganic materials (*e.g*: silicon) which not only lead to high efficiency, but also high cost. This is the main solar cells and silicon carries on to rule in the marketable market because of its dominant qualities. The second generation of solar cells was established with the aim of to cut the high costs dominant in the first generation over the utilization of the thin film technology. The awareness on reducing the cost with the important reduction in the quality of the materials and the challenge of increasing the thin film absorption to compensate for reducing the thickness of photoactive layers (Stintzing & Carle, 2004).

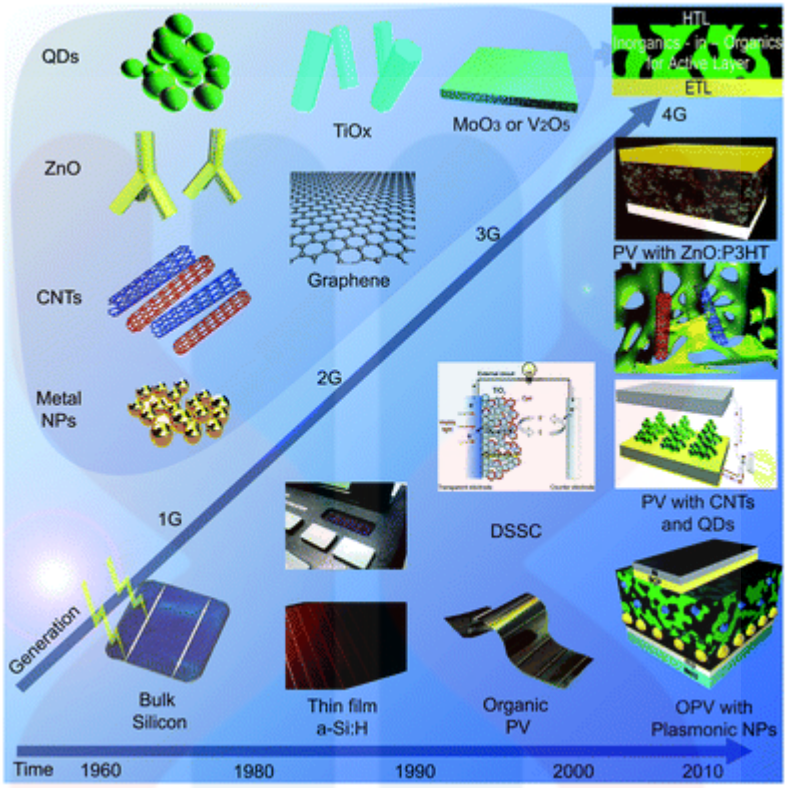

Figure 2.1: Various solar devices (Jonathan *et al*., 2016)

This second generation (2G) thin film technology was established on the solar cell materials recognized during the improvement of first generation solar cell and was prolonged to include the amorphous or polycrystalline amorphous silicon (a-Si), copper indium gallium selenide (CIGS) and cadmium telluride (CdTe). The second generation solar cells addresses the cost matters associated with the thick films, yet the performance of such second generation of solar cell is still poor compared to the first generation counterpart.

Therefore, the task was to expand the efficiency as much as possible within the reasonably priced materials, to compensate for the considerably reduced the active volume. Intrinsic layer was developed to produce p-i-n devices where photogenerated carriers should be removed to the doped materials by the built-in field. The main factor for this second generation solar cell was the cost per watt transfer, but the requirement for the extended surface areas to compensate for the lower efficiency was become the issues. Hence, this in turn to the improvement of the third generation of solar cell (Jonathan *et al*, 2016; Krebs *et al*, 2013).

Thereafter, researchers have been focused on the design of nanoscale materials and scale-up to the macroscopic regions. For the first time, significant consideration was funded to the charge and energy transfer processes and the particular routes to improve charge collection, in that way enhancing the energy capture within the solar spectrum. With the overview of organic materials showing photovoltaic properties, their potential for low cost and high optical absorption placed them as a third generation technology. In addition to organic (or polymer) solar cells, additional candidate that dominates third generation (3G) solar cell technologies is dyes-sensitized solar cells (DSSCs) (Kazici *et al*., 2018).

Regardless of the practical success of the 3G cells, the improvement in device performances are still compulsory in order to be reasonable with the previous solar cell generations in terms of cost per watt. The various types of solar cells introduced in this generation, basically in using of innovative semiconductor such as nanocrystal solar cells, photoelectrochemical (PEC) cells, Gräetzel cell, dye sensitized hybrid solar cells and polymer solar cells.

PECs were next on the lists which consist of semiconducting photoanode. It workings best with electrons and can also isolated the non-salacity of semiconductors. Gräetzel cells or also known as dye sensitized used photoelectrons to increase power efficiently. Dyes were made of metal organic complex and its molecules are success by increasing heat. The polymer solar cells were the last invention of this generation, posses the properties of lightweight, inexpensive, flexible, and disposable at any molecular level. In turn, these third generation solar cells offer significant cost improvements on first and second generation solar cells.

The fourth generation (4G) of solar cell technology conglomerates the low price/flexibility of polymer thin films with the stability of novel inorganic nanostructures to improve the photoelectronic properties of low-cost thin film solar cell. These device architectures are meant to sustain the low-cost nature of a solution-process able solar cell device structure, but include inorganic components to increase on energy harvesting cross-sections, the charge dissociation, and charge transport within the solar cells. Mesoscopic solar cells can be considered as a 4G technology due to the assimilation of an inorganic component (e.g: titania), especially when mutual with a polymer or organic layer as a solid-state DSSC. To date, the most operative polymer solar cells (PSCs) were reported based on the bulk heterojunction (BHJ) concept.

The 4G solar cells are a hybrid that combines the low price and flexibility of conducting polymer films (organic materials) with the generation stability of novel nanostructures (inorganic materials). This inorganics-in-organics technology increases the gathering of solar energy and its alteration into electricity, present well efficiency than the current 3G solar cells while sustaining their low cost base. These new generation materials

for solar cells have been truly planned at the nanoscale. They are planned to get the best out of the harvesting of solar radiation, and thereby efficiently produce electricity. It is believed that 4G solar cells will be the technology for future photovoltaic energy sources. This generation takes most successful types of solar cells for mankind and those were hybrid-nanocrystal cells. For generation of these cells polymers and nanoparticles were mixed to make on layer which can help electrons and protons to transfer for generating better voltage and good quality of direct current (Mohammad, 2015).

2.3 Dye-Sensitized Solar Cell

Solar energy conversion has been widely studied for many years, but in latest years, dye-sensitized solar cell (DSSC) have become an attractive renewable energy alternative. In 1991, Michael Gräetzel and Brian O'Regan presented the innovative photovoltaic device to the scientific public that required a very modest means of production that permitted for low-costing and moderately efficient solar cells. DSSC belongs to the 3G photovoltaic cells that uses molecules to absorb photons and split up the two functions of light harvesting and charge transport. As one of the best significant advantages of this type of solar cells is their suitability for numerous materials, and the possibility of the production under mild conditions, making it significantly less expensive than other kind of solar cells. DSSCs are made in a sandwich configuration of conducting glass. Figure 2.2 presented the schematic illustration of DSSC.

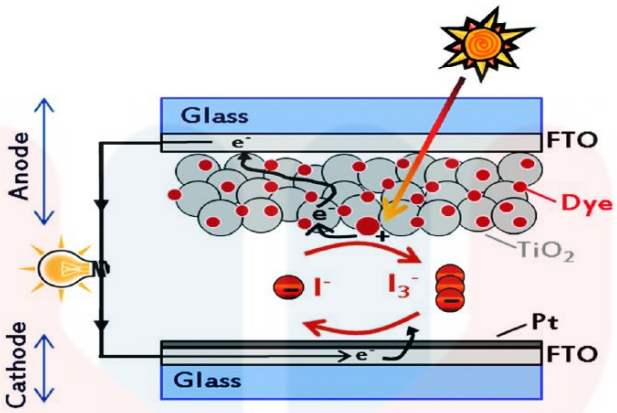

Figure 2.2: A schematic representation of a DSSC (Bella *et al*., 2015)

The main components of DSSC are a wide band gap semiconductor to which the dye is absorbed and placed on the transparent electrode (photoanode), electrolyte with a redox mediator and a counter-electrode. The sandwich structure of DSSC includes two transparent conducting glass substrates. In this situation, the front side illumination where the glass substrate acts and act as a window for the incident light which consequently be extremely translucent in the visible-IR region (Fujishima *et al*., 2007). Blocking UV light might be preferred to inhibit the photodecomposition of the dye due to bad gap excitation of the semiconductor.

The substrate of the electrode helps as a collector for the current and it is fine transparent conductor. On the other hand, the backside illumination through the counter electrode would have a reflecting photoelectrode substrate to boost light absorption by reflecting back the transmitted light into the dye. The substrate is also act as the perfunctory provision for semiconductor coating, which must powerfully adhere to it. An additional requirement used for the substrates is a low sheet resistance which is temperature self-

regulating to the high temperatures (*e.g*: 450 - 500 °C) used for the TiO_2 sintering (Mazhdi *et al*., 2013).

A semiconductor is a material in which little concentrations of charge transferors can be created either by thermal or photo-excitation, or by chemical doping. Essential semiconductors are categorized by a totally occupied valence band and an unoccupied conduction band. Essential absorption of photons, whose energy is greater than the bandgap, creates electron-hole pairs. DSSC uprising happening essentially from the solicitation of the mesoporous TiO_2 layer be made up of 20 nm sized nanoparticles (Oprea *et al*., 1991). Some metal oxides such as TiO_2, SnO_2 or ZnO with energy band gap greater than 3 eV do not absorb visible light that have been studied as potential electron acceptors for DSSCs.

DSSC was reported little efficiency of less than 1% until Gräetzel employs porous TiO_2 as the anode material. Titanium dioxide (TiO_2), a n-type semiconductor through a wide bandgap and widely used as photoanode of DSSCs. It proposals particular exclusive properties making it the number one semiconductor for DSSCs. Its conduction band edge lays to some extent lower the excited state energy level of many dyes, which is one of the situations for effective electron injection. In 1985, Desilvestro demonstrated that if TiO_2 is used in a nanoparticle form, the power conversion efficiency of DSSC can be extremely improved.

In line for to the wide bandgap of TiO_2, it absorbs the photons up to 390 nm. So that in order to produce as greatly as possible of the solar spectrum, dye molecules which chemically bound to the TiO_2 surface acting as antennas. In order to choose a dye molecule

nearby are, a few criteria takes to be achieved to make assured that the sensitization happens efficiently. Such as, the dye must have a extensive absorption spectrum, in order to detention as much as possible of the solar radiation. In addition, the extinction coefficient (ε) of the dye must be extraordinary above the whole absorption spectrum, to engross greatest light with a minimum of dye and the excited state of the dye commitment powerfully lie exceeding the conduction band edge of the semiconductor, to guarantee fast electron injection.

In addition, the enthusiastic state generation of the dye necessity is long enough for well-organized electron injection and the oxidized dye need to make sure that more positive potential than the redox couple in the electrolyte, to inhibit recombination of the injected electron with the oxidized dye. On the other hand, the redox potential of the electrolyte should be rather positive, meanwhile it regulates the impending of the counter electrode and so the photovoltage of the cell.

Moreover, the dye essentials assigning groups such as $COOH^-$, $H_2PO_3^-$ and SO_3H^- to increase the chemical bonding with the semiconductor surface and to work as channels for electron injection. Dye also has to be soluble in some solvent for better adsorption on the electrode, and do not be desorbed by the electrolyte redox.

The electrolyte acting as a very significant role in the DSSC by helping the transport of charge stuck between the working and counter electrodes. The electrolyte role is to stimulate the oxidized dye and for the transmission of the positive charge to the counter electrode, where the redox-couple itself is regenerated by an electron flowing back through the external circuit. Nonetheless, various features are essential in place of some electrolyte

such as, the redox-couple need to be alterable at the counter electrode and not respond on the TiO_2 electrode. In addition, the electrolyte must not engross intensely in the visible spectrum and on the other hand, the redox potential has to be as positive as possible, in the meantime the open circuit voltage is determined by on the potential of the counter electrode and the electrolyte.

The counter electrode is another alternative critical component in DSSC anywhere the mediator is compact. The function of the counter electrode is to transmission of the electrons incoming from the external circuit back to the redox electrolyte. Henceforth, it needs to be well conducting and exhibition small voltage for reduction of the redox couple. In addition, it might work for as mirror, imitating the light transmitted by the photoelectrode to pass through it a second time, thus increasing light absorption with a generous quantity of dye. Examples of counter electrode are platinum, graphite and aluminium (Kay & Gräetzel, 1996).

2.4 Natural Dye Sensitizer

Naturally available fruits, flowers, leave and bacteria exhibit various colors and contain several pigments that careported widely in the application of dye-sensitized solar cell (DSSCs) (Chang & Lo, 2010). The advantages of applying natural dyes are due to their large absorption coefficients in visible region, relative abundance, ease of preparation and environmental friendliness (Gómez-Ortíz *et al*., 2010). Most importantly, the synthesis route for these type of material is cost effective and toxic-free which it does not involve noble metals like ruthenium (Ru) (Maldonado *et al*, 2013).

The plant pigments exhibit electronic structure that interacts with sunlight and alters the wavelengths that are either transmitted or reflected by the plant tissue. This process leads to the occurrence of plant pigmentation and each pigment is described from the wavelength of maximum absorbance and the color perceived by humans. Typically, pigments of natural dyes such as chlorophyll, carotenoid, flavonoid and betacyanin were widely reported due to its relatively easy to extract from natural products (Kumara *et al*., 2013).

Betalain is another interesting class of pigments, whose purified extracts from commercial sources have been subjected to photoelectrochemical study (Fang, Xing, & Zhang, 2017). Betalains consisting of the yellow betaxanthins and red–violet betacyanins are a group of water-soluble nitrogen-containing alkaloid pigments characteristic of certain members of plant sub-order chenopodineae within caryophyllales and some higher fungi (Nivea *et al*., 2014). They absorb visible radiation in the range from 476 nm to 600 nm, represent as immonium derivatives of betalamic acid that have a maximum absorptivity at $\lambda \approx 535$ nm (Kumara *et al*., 2013).

Betalains are characterized by high molar extinction coefficients in the visible region and pH-dependent redox properties which relatively stable for pH 3 until pH 7, however, less then pH 3.5, the absorption maximum shifts toward lower wavelength (Hernandez-Martinez *et al*., 2011). Acidic conditions are known to induce recondensation of betalamic acid with amine group of the addition residue and favors betalain-sensitized photo-electrodes with high optical densities capable of complete absorption in the visible range of 400 nm – 600 nm (Calogero *et al*., 2010).

In this work, the betalain pigment extracted from *Hylocereus polyrhizus sp*. (dragon fruit) flesh was applied as natural dye sensitizer in dye-sensitized solar cell (DSSCs). Generally, betalain stability was influence greatly by light. It has been reported to deteriorate betalain stability (Herbach *et al.*, 2006). The betalain pigment of dragon fruit is varied based on sources due to the presence of saccharide type present in the betanidin (Isah *et al*., 2012).

The chemical structure of betalain contains carboxylic functional group that make bonding with metal oxides surface binding. This can be shown in Figure 2.3.

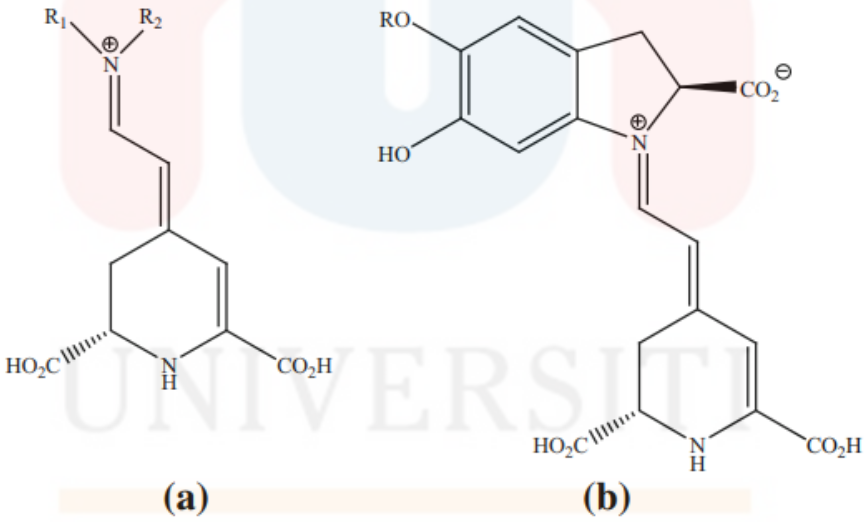

Figure 2.3: Chemical structure of the main betalain which (a) Betaxanthin (R_1 = H and R_2= amine) and (b) Betacyanin (R = β-D-glucose) (Strack, Vogt, & Schliemann, 2003).

2.5 The Energy Bandgap

Federico was implied the application of band gap engineering in semiconductor devices in late 1980s. He recommended the idea of band gap engineering, which is the band diagram of semiconductor, that can be custom-made and the carriers transport can modified for specific application with the assistance of heterojunction and modern growth method. The concept has been developed and has modified for various field application, such as for graded gap transistor, carbon nanotube/grapheme and nanocrystal. For example, the band gap of nanocrystal can be modified based on modification in alloying, doping, strain tuning and band gap edge warping (Fujishima *et al*., 2007)..

Based on the typical dye-sensitized solar cell (DSSCs) mechanism, the photons strike the dye on the titanium dioxide (TiO_2) which the energy will be absorbed by the dye and produce the excited state of dye. The excited state dye will inject electron directly to the conduction band. The injection of the electron would be more efficiency if the range between the valence band and conduction band is short (Oviri & Ekpunobi, 2013). Figure 2.4 show the illustration of bandgap mechanism. The quantized energy levels detected in quantum dots lead to electronic structures that are intermediary concerning single molecules which have a single HOMO - LUMO gap and bulk semiconductors which make sure continuous energy levels within bands (Fujishima *et al*., 2007).

Between the valence and conduction band, there is an energy bandgap, which is used in determining material ability in conductivity. The value of the bandgap energy of certain dye will influenced the transition of the electron between the valence band to

conduction band and resulted conductivity rate (Syafinar *et al*., 2015). Therefore, when the bandgap is smaller, the conductivity will be higher. As the less energy needed for transition between the HOMO and LUMO, the more current can be produced in the DSSC (Kantesaria, 2014).

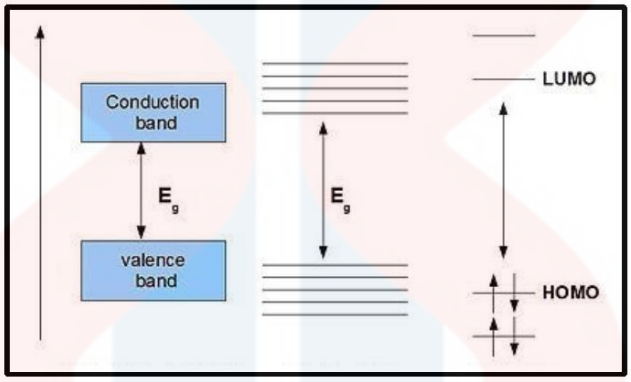

Figure 2.4: Illustration of the bandgap mechanism (Ayalew *et al*., 2016)

There are two energy levels in dye pigment which are highest occupied molecular orbital (HOMO) and lowest unoccupied molecular orbital (LUMO) levels in DSSC. The lowest energy transition is that between the HOMO and LUMO in the ground state. HOMO and LUMO level of sensitized play an important role in photo generation, electron injection, dye regeneration and power generation of device. The more exceedingly conjugated the system, the smaller the HOMO-LUMO gap.

CHAPTER 3

MATERIALS AND METHODS

3.1 Materials and Apparatus

The chemicals that were used in this study including titanium dioxide nanopowder (TiO_2) from (Aldrich), aluminium oxide (Al_2O_3) (Bendosen), zinc oxide (ZnO) (Bendosen), glass detergent (Decon 90), acetone, potassium iodide crystal, acetonitrile, propylene glycol, ethylene glycol, ethanol, methanol and 2-propanol. The natural plant-derived dyes was extracted from *Hylocereus polyrhizus sp*. (dragon fruit) flesh that was collected from fresh market in Jeli, Kelantan.

Few apparatus also were used in this study, which are indium tin oxide glass (ITO), magnetic stirrer, sample bottle, beakers, filter papers, mortar and pestle, spatula, adhesive tapes, hair dryer, petri dish, aluminium foil, microscope glass, cuvette, measuring cylinder,

knife, clipper, gloves, furnace, water bath, centrifugation machine, oven dry, hot plate, dehydrator, a set of vacuum pump, digital multimeter and ultrasonic cleaner.

3.2 Equipments

To complete this study, several analysis were carried out to analyze the dye extract and solar devices includes ultraviolet-visible spectrophotometer (UV-vis) (HACH DR600), scanning electron microscopy (SEM) (Jeol JSM-IT100), four point probe (4PP) (Jandel HM21 1.3) and electrochemical impedance spectra (EIS) (Metrohm Autolabs).

3.3 Methods

3.3.1 Preparation of Natural Dyes Extracts

The preparation of natural dye extracts was done based on the literature with some modifications (Jonathan *et al*., 2016). *Hylocereus polyrhizus sp*. (dragon fruit, **DF**) was collected from fresh market in Jeli, Kelantan. Firstly, 1 kg of **DF** was washed with distilled water and dried using dehydrator for 48 hours to remove excess water. The dried samples were then grinded using dry blender to make it into powder form which then, stored with no exposure to the light. Next, 120 g of fresh **DF** flesh were cut into small pieces and soaked in 120 ml methanol absolute and properly stored at room temperature under dark condition for overnight. After that, the fleshes of **DF** are mash using pastel and mortal.

Finally, the solution was then filtered using 0.45 µm Whatman filter paper with the aid of a set of vacuum pump. Figure 3.1 shows the photos of extract dye solution from **DF**. The natural dye extract was then properly stored in the dark condition at 16 °C upon further characterization.

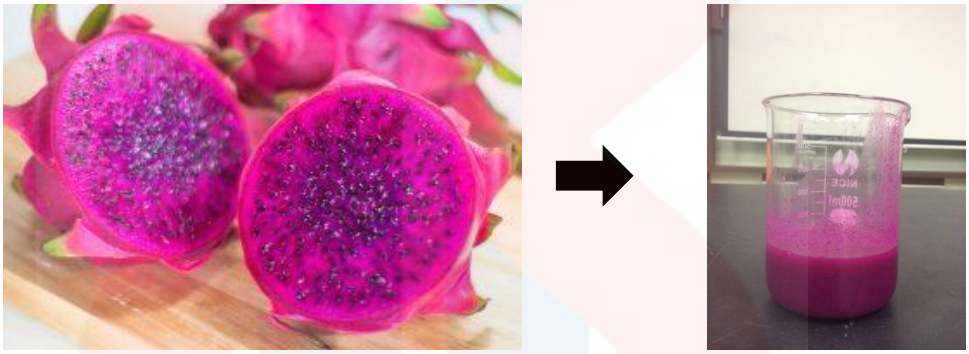

Figure 3.1: The samples of *Hylocereus polyrhizus sp*. (dragon fruit) before and after extraction.

3.3.2 Preparation of Metal Oxide Paste Solution

3.3.2.1 Aluminium Oxide, AO

Al_2O_3 paste was prepared by dissolving 2.6 g of Al_2O_3 powder into 100 ml of methanol and stir for 4 hours until homogeneous paste solution was obtained. The paste formed was placed in the dark room and ready for the preparation of Al_2O_3 thin film.

3.3.2.2 Titanium Oxide, TO

TiO_2 paste was prepared by dissolving 2.0 g of TiO_2 nanoparticles into 100 ml of ethylene glycol and stir for 30 min until homogeneous paste was obtained. Subsequently, 1 ml of the prepared TiO_2 paste was mixed with 100 ml of ethanol. The TiO_2 paste solution was placed in the dark room and ready for the preparation of TiO_2 thin film.

3.3.2.3 Zinc Oxide, ZO

ZnO paste was prepared by dissolving 2.0 g of ZnO powder into 100 ml of methanol and stir for 4 hours until homogeneous paste solution was obtained. The paste formed was placed in the dark room and ready for the preparation of ZnO thin film.

3.3.3 Preparation of Electrolyte

1.1 g of potassium iodide crystal was dissolved into the mixture solvent of 20 mL and 5 mL of acetonitrile and ethylene glycol respectively. Subsequently, 0.35 g of iodide crystal was added into the solution and allowing them stirring for 30 minutes until the homogeneous solution was obtained. The solution formed was place in the dark room and ready for the fabrication proses.

3.3.4 Preparation of Carbon Black Counter Electrode

For the preparation of carbon counter electrode, the cleaned-ITO glass were coated with carbon black resulted from passing the candle flames to form candle soot, as shown in Figure 3.2.

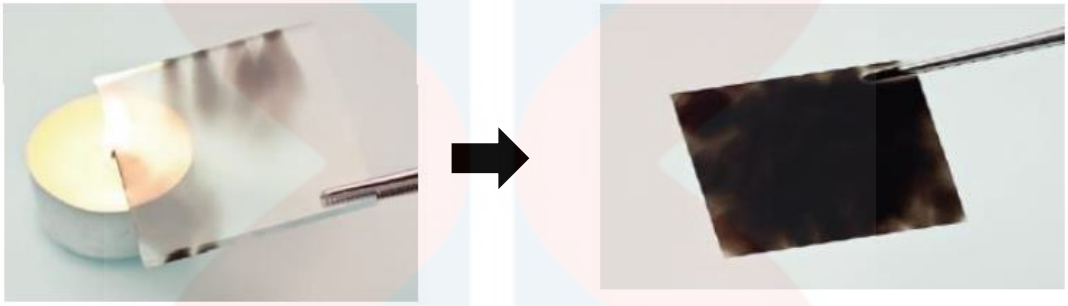

Figure 3.2: The carbon on ITO glass to prepare counter electrode, before and after carbon coating.

3.3.5 Fabrication of Dye-Sensitized Solar Cells

ITO conductive plates were cut into 2 cm × 2 cm pieces. All ITO glasses were cleaned using Ultrasonic cleaner at 50 °C. The cleaning process was started with distilled water followed by DECON 90 detergent and rinsed with distilled water, ethanol and 2-Propanol. Subsequently, ITO glasses were placed in the beaker filled with the solvent and the beaker was then inserted in the removal basket inside the ultrasonic cleaner which was filled with 50 °C of tap water. The level of the solvent in the beaker was totally immersed under the level of tap water. The glasses were placed with ITO layer facing up the bottom of beaker during the process for an optimal cleansing. Each solvent was set for 15 minutes cleansing process respectively. DECON 90 detergent was used as a solvent to break down

the surface tension of water base and to cavitate efficiently. The temperature of tap water in the ultrasonic cleaner tank was continually observed to avoid it reaching 78 °C, the boiling point of ethanol where at that state the intensity of cavitation stops. The excess water on the ITO glasses was instantly dried out by using hair dryer. Metal oxide (**TO**, **AO**, **ZO**) paste was then deposited on the ITO surface by using doctor blade technique and left to dry on the hotplate at 70 °C for 15 minutes. Next, the ITO glasses are then sintering at 500 °C for 30 minutes ramp time. The sintered metal oxide (**TO**, **AO**, **ZO**) films were dyed with natural dye extracts of *Hylocereus polyrhizus sp*. (Dragon fruit) (**DF**) for overnight at room temperature under dark condition. The dyed – **MO** electrode and carbon black counter electrode were assembled with the presence of few drops of electrolyte between both ITO glass. The clip was holding both edges of ITO glass and the device ready for solar cell measurement. Figure 3.2 summarizes overall procedures involved in the fabrication of completed dye-sensitized solar cells (DSSCs).

ITO glass was prepared.

The ITO glass was cleaned in detergent solution, rinse with water and ethanol before drying process.

The **MO** paste was prepared.

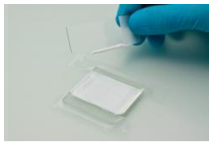

The **MO** paste was coated on the ITO glass by doctor blade technique.

MO/ITO glass film was sintered at 500 °C for 15 minutes.

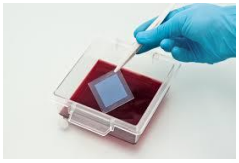

MO/ITO glass was immersed in extracted dyes solution (**DF**) for overnight.

Preparation counter electrode by deposition of carbon soot from a burning candle.

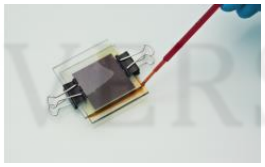

MO/ITO glass film and counter/ITO glass were assembled to form complete device and filling with electrolyte.

Several analysis were conducted to evaluate its potential in solar cell application.

Figure 3.3: The fabrication of **MO**/**DF**/carbon for dyes-sensitized solar cells, which **MO** = TiO_2, Al_2O_3, ZnO and **DF** = Dragon fruit.

3.4 Characterization

The absorption spectra of *Hylocereus polyrhizus sp*. (dragon fruit, **DF**) were determined using UV-Vis spectrophotometer (Spectrophotometer HACH DR 6000) in the wavelength range of 400 nm to 800 nm. From the absorption spectra, the bandgap energy of dye was evaluated by using Tauc-plot method. The surface morphology of **DF** on indium tin oxide (ITO), titanium oxide (TiO_2, **TO**) nanopowder, aluminium oxide (Al_2O_3, **AO**) and zinc oxide (ZnO, **ZO**) were observed using JEOL JSM IT 100 Scanning Electron Microscope (SEM) at 200 ×, 300 × and 1000 × of magnification. The conductivity of solar cell devices was measured using four point probe (4PP) and the short-circuit photocurrent (I_{sc}), open-circuit voltage (V_{oc}), fill factor (FF) and power conversion efficiency (PCE) were measured using electrochemical impedance spectroscopy (EIS).

CHAPTER 4

RESULTS AND DISCUSSION

4.1 Physical Observation of Extract Dye Solution

In this study, the dye-sensitized solar cells (DSSC) were prepared using natural fruit dye extracted from *Hylocereus polyrhizus sp*. (dragon fruit, **DF**) as photo-sensitizer. **DF** was being chosen as a source of dye, which from its color is predicted to have appropriate optical absorption. **DF** also was chosen due to the presence of the natural occurring betacyanin of betalain pigment which are responsible for the red, violet and purple coloration in the most species of plant kingdom (Florian & Reinhold, 2004). The color of the dye extracted from **DF** was physically observed. Figure 4.1 shows the image of the **DF** dye.

(a) (b)

Figure 4.1: **DF** solution during the extraction where (a) **DF** solution prepared and (b) **DF** solution after filtration.

From the physical observation, it can be identified that the color of **DF** in methanol was in purple solid color. The degradation of dye extract is highly depends on the temperature of preservation and the exposure of dye extract to the light. Betacyanin, which the pigment in **DF** was stated as sensitive to heat, pH, light, moisture and oxygen. In 2016, Abdel-Latif stated that the heat treatment is not exceeding over 60 °C and better to store at 4 °C.

4.2 UV-Vis Absorption Spectrum Analysis

Absorption spectrum analysis is use to determine the potential materials for the photosensitizer layer in dye-sensitized solar cell (DSSC). Thus, in this study, UV-Vis is used to observe the ability of dye in photo-absorbance properties and also can determined the specific peak in solar spectra region that will give a result of particular dyes compound present in the dye pigment.

4.2.1 *Hylocereus Polyrhizus* (dragon fruit, DF)

UV-Vis absorption (HACH DR600) was used to evaluate the photo absorption properties of single **DF** dye solution. The UV-Vis absorbance range was set at the 400 nm to 800 nm. From the UV-Vis spectra shown in Figure 4.2, the absorption spectra of **DF** dye was identified.

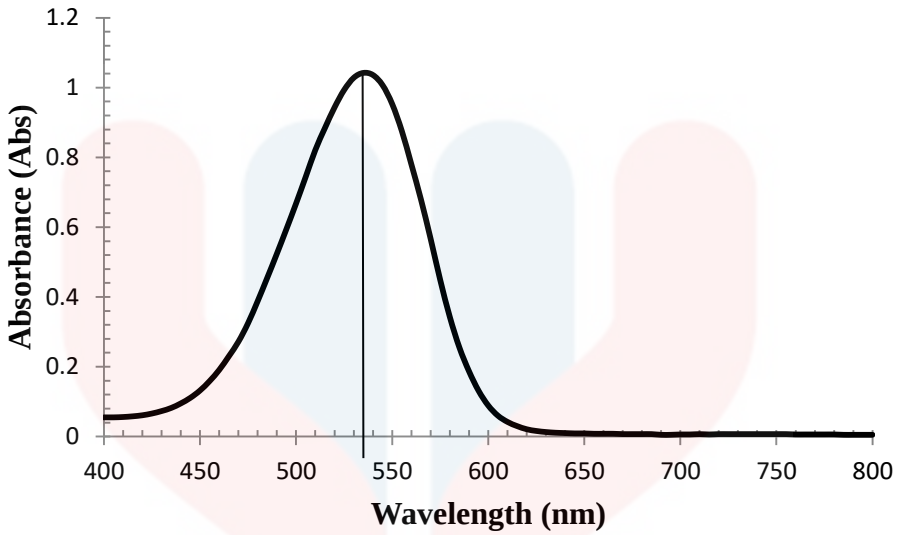

Figure 4.2: Absorption spectra of *Hylocereus polyrhizus sp*. (dragon fruit, **DF**).

The dye compound of **DF** has showed the peak absorption at 535 nm, which almost same as reported previously, represent the absorption of betacyanin with absoption range from 450 nm to 600 nm (Woo *et al*., 2011). From the result, it is understood, that **DF** will absorb light range from 450 nm to 600 nm. Thus, **DF** showed good absorption in visible light region which can utilized more photon energy between 400 nm to 600 nm. From the result obtained, betacyanin pigment would carry out the absorption of light from 450 nm to 600 nm wavelength (Ahmad *et al*., 2010) (Jonathan *et al*., 2016).

4.2.2 Metal Oxide

UV-Vis absorption (HACH DR600) was used to evaluate the photo absorption properties of **DF** on ITO and metal oxide (**MO**) on ITO glass in visible

region of wavelength from 400 nm to 800 nm. The absorption spectra of **MO** was shown in Figure 4.3.

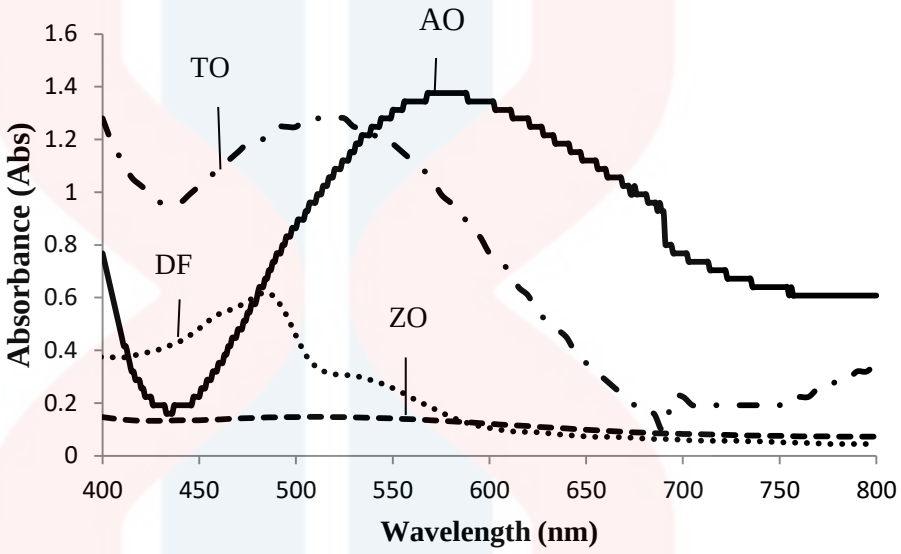

Figure 4.3: Absorbance spectra of **DF**/ITO and **MO**/ITO (**MO** = **TO**, **AO** and **AO**).

From the UV-Vis spectra shown in Figure 4.4, the absorption spectra of **MO**-**DF** coated on ITO glass was identified. **DF** coated on ITO glass has the absorbance peak at 490 nm wavelength with absorbance of 0.38 (<1) which means that it exhibits good absorbance at UV region (Viezbicke *et al*., 2015). These peak are located in the region of betalain pigment that presence naturally in **DF** (Woo *et al*., 2011).

From the Figure above, we can see that **TO** has the region of absorbance range from 450 nm to 650 nm, while **AO** has the absorbance range from 450 nm to

700 nm and the region of absorbance range of **ZO** is in the range of 500 nm to 600 nm respectively.

Beside, UV-Vis absorption (HACH DR600) also was used to evaluate the photo absorption properties of **DF** on ITO and metal oxide (**MO**) with dyes-coated (**MO**/**DF**) on ITO glass in visible region of wavelength from 400 nm to 800 nm. The absorption spectra of **MO**/**DF** was shown in Figure 4.4.

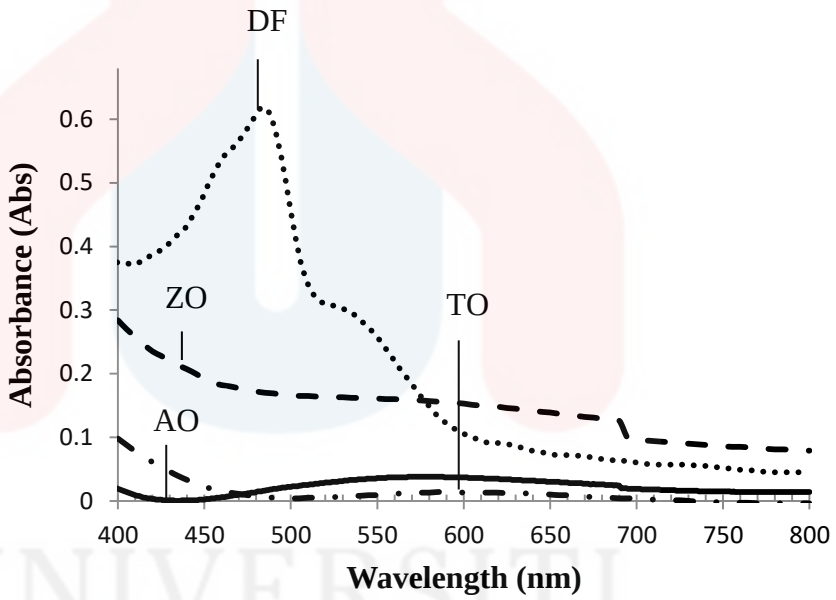

Figure 4.4: Absorbance spectra of **DF**/ITO and **MO**/**DF**/ITO (**MO** = **TO**, **AO** and **AO**).

From the UV-Vis spectra shown in Figure 4.5, the absorption spectra of **MO**-**DF** coated on ITO glass was identified. **DF** coated on ITO glass has the same value that recorded previously.

The ability of betacyanin in individual **DF** is not good enough. Hence, in this study the introduction of **MO**/**DF**/ITO was introduced which led to an effective reaction for a better absorption spectra. From the broad spectrum observed in Figure 4.4, the significant peak for **TO** was observed at 530 nm wavelength with absorbance of 0.03 (<1).

4.3 Bandgap Measurement

4.3.1 *Hylocereus Polyrhizus* (dragon fruit, DF)

A bandgap is the expanse among the valence of electrons and the conduction band. Principally, the band gap exemplifies the minimum energy that is compulsory to excite an electron up and about to a state in the conduction band where it can contribute to the conduction (Bella *et al*., 2013). The lower the energy level is the valence band, therefore if a gap exists between this level and the higher the energy conduction band, the energy necessity to be input for electrons to become free. Band gap energy is applied to determine the qualitative analysis of the absorption spectrum obtained from the UV-Vis spectrophotometer.

Tauc method is an optical absorption edge value (λ edge, in nm) determination as direct bandgap materials by using simple multi-wavelength absorption spectroscopy using following equation that summarized in Table 1 (Viezbicke *et al*., 2015). The Tauc optical gap is determined over and done with an extrapolation of the liner trend detected in the

spectral dependence of $(\alpha hv)^{½}$ over a restricted range of the photon energies h*v* (Mok *et al*., 2007).

Table 4.1: Tauc model to calculate the bandgap of materials (Viezbicke *et al*., 2015).

Bandgap Energy (E) = hc/λ				
Planck's constant (h) = 6.63×10^{-34} Joules sec				
Speed of light (c) = 3.00×10^{8} meter/sec				
Cut – off wavelength (λ) = 420.57×10^{-9} meters				
H	C	λ	E	eV
6.63 E–34	3.00 E+08	From UV-Vis	From calculation	From calculation
Where 1 eV = 1.6×10^{-19} Joules (conversion factor)				

In this study, the energy difference between the energy level of materials in DSSC is equally understand the concept of electron transport upon the photon energy excitation. The bandgap energy determination will aid in the structural arrangement of the layer depending on the bandgap energy obtained.

Figure 4.5 shows the plotted peak of energy derived from the UV-Vis spectra and Tauc plot measurement of **DF**. The estimation of the optical bandgap was made based on the intersection of the dashed line with the x-axis. In this study, the bandgap energy was determined at 540 nm. At 540 nm, the bandgap energy of the betacyanin pigment from **DF** was recorded of 2.15 eV. The photon from sunlight is used to excite electrons from a lower energy level (HOMO) transfer to the conduction band of a wide bandgap (LUMO).

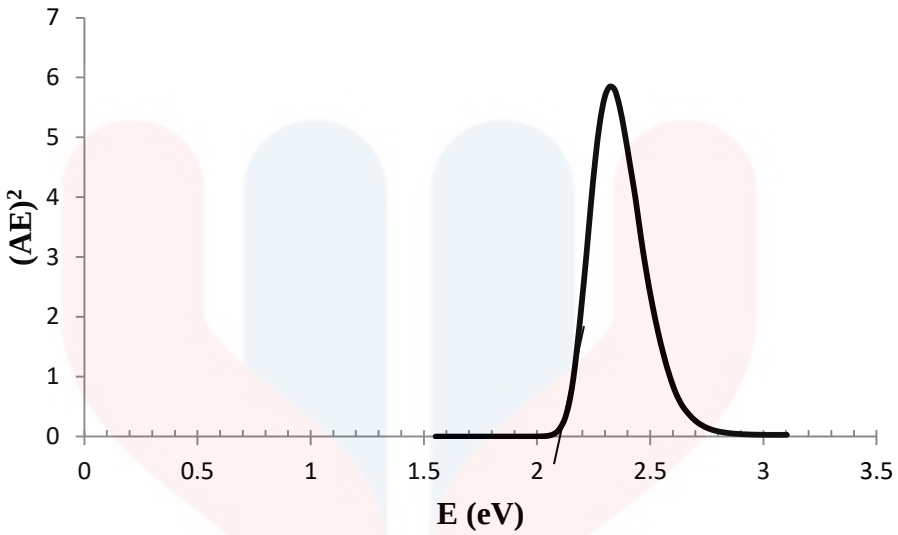

Figure 4.5: Bandgap energy determined from Tauc Plot measument

4.3.2 Metal Oxide

There are three differences of metal oxide (**MO**) that were prepared in this study which are titanium oxide (**TO**), aluminium oxide (**AO**) and zinc oxide. Figure 4.6 shows the difference bandgap energy of metal oxide (**MO**) coated on indium tin oxide (ITO). The distinct difference occurred in the **TO** since the bandgap energy attained was 2.75 eV followed by **ZO** at 2.65 eV and **AO** at 2.96 eV respectively.

From the analysis, the value of the bandgap energy levels shows that **AO**/ITO has the highest bandgap energy followed by zinc oxide **ZO**/ITO and aluminium oxide **TO**/ITO. The greater the difference between the bandgap energy, the lower the energy conversion. The small crystalline size make **TO** nanoparticles to be potentially used as electrode in solar cells compared to **ZO** and **AO**. In this study, the bandgap value of **ZO** is 2.65 eV,

which is lower than reported value 3.53 eV (Mazhdi *et al*., 2012). The decrease in bandgap of **ZO** with large particle size may be due to a quantum confinement effect (Kazmi *et al*., 2016).

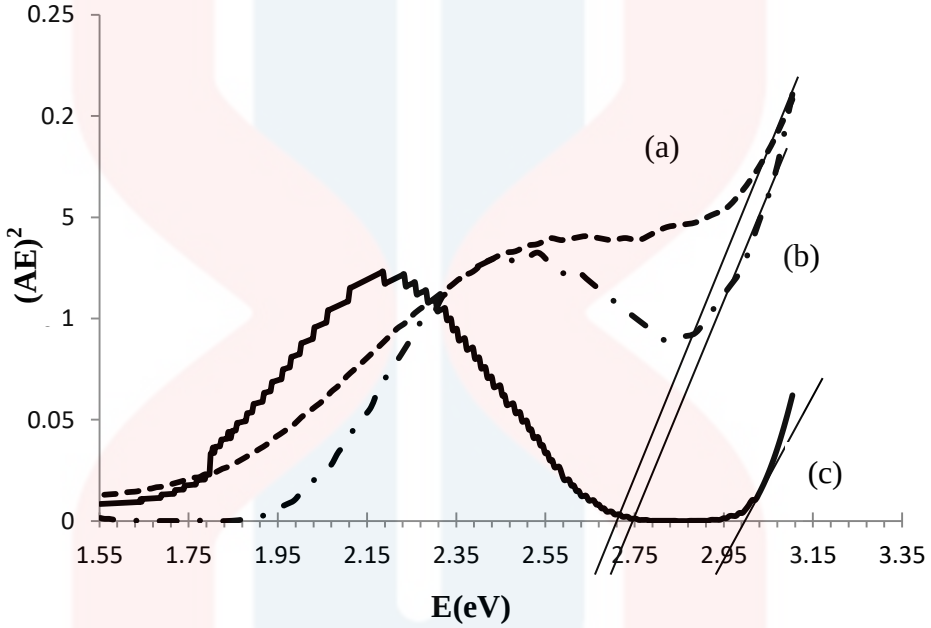

Figure 4.6: The bandgap energy of **MO**/ITO determination from Tauc Plot of (a)**ZO**/ITO = 2.65 eV, (b) **TO**/ITO = 2.75 eV and (c) **AO**/ITO = 2.96 eV.

Meanwhile, Figure 4.7 shows the difference bandgap energy of metal oxide (**MO**) coated on *Hylocereus polyrhizus sp*. (dragon fruit, **DF**) on the indium tin oxide (ITO) (**MO**/**DF**/ITO). The distinct difference occurred in the **TO**/**DF**/ITO since the bandgap energy attained was 1.55 eV followed by **ZO**/**DF**/ITO at 2.60 eV and **AO**/**DF**/ITO at 2.80 eV respectively compared to the bandgap energy value of **TO**/ITO, **ZO**/ITO and **AO**/ITO which are 2.75 eV, 2.65 eV and 2.96 eV respectively.

In this study, **TO**/**DF**/ITO has the lowest bandgap energy which is 1.55 eV followed by **ZO**/**DF**/ITO and **AO**/**DF**/ITO. In order to achieve a good efficiency, one of the reason should because of the dye use. The **DF** dye must bind strongly to the substrate. The standard anchoring moiesties for the sensitizers are the carboxyl group (-COOH), which will bind to **TO** in a bridging mode (Oprea *et al*., 2013). The **TO** nanoparticle has the physical properties which are dominated by the special confinement that manifests itself in widening of HUMO and LUMO gap or the bandgap increase with the decreasing of crystallite size (Fujishima *et al*., 2007).

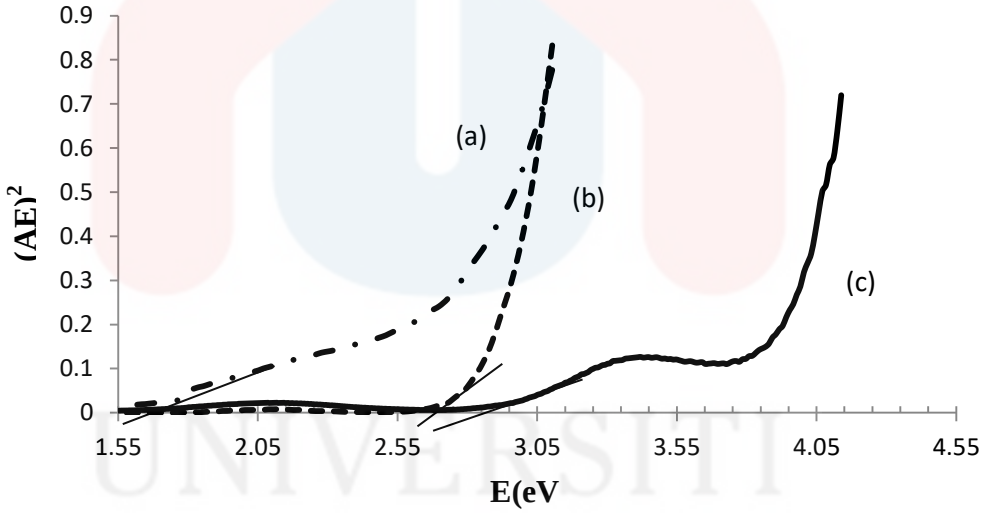

Figure 4.7: The bandgap energy of **MO**/**DF**/ITO determination through Tauc Plot. Where (a) **TO**/**DF**/ITO = 1.55 eV, (b) **ZO**/**DF**/ITO = 2.60 eV and (c) **AO**/**DF**/ITO = 2.80 eV.

4.4 Scanning Electron Microscopy Analysis

SEM is one of the most frequently used microscopy technique in material structure analysis. It can make available high resolution image of the materials, up to 1 to 5 nm, and clear 2D structure with the microscopes's large depth of field. SEM was first developed by Max Knoll in 1935 but the actual SEM machine was actually build by Sir Charled Oatley from late 1940s to 1967 (Genc *et al*., 2015).

Morphology of the *Hylocereus polyrhizus sp*. (dragon fruit, **DF**) powder, metal oxide (titanium oxide (**TO**), aluminium oxide (**AO**), zinc oxide (**ZO**)) powder was viewed with different magnification. Figure 4.8 shows the picture of **DF** coated on ITO glass. The morphology of **DF** on ITO glass formed clusters of small holes structure with large surface area by having average size of 100 µm using 200 x of magnification. The image of clusters of small holes obtained was found in similar image reported previously about dragon fruit extracts (Priyantha *et al*., 2015).

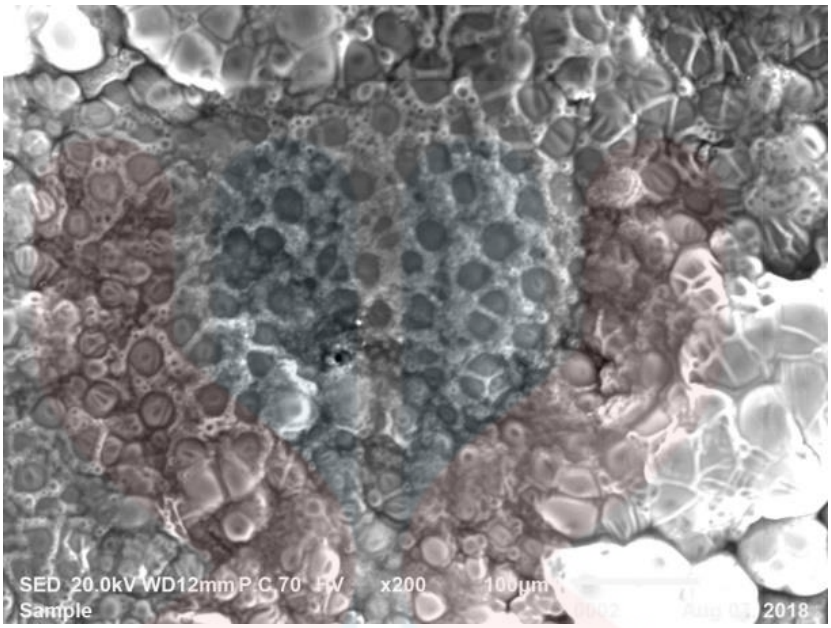

Figure 4.8: The morphology of **DF**/ITO glass.

Meanwhile, the morphology of **TO**/**DF**/ITO was presented in Figure 4.9, with the magnification of 1000 x and the size of porous are 10 µm. It can be seen that there was no agglomerations of particles and the particle distribution is uneven and white particles on the image are **TO** nanoparticles (Tahir *et al*., 2018). The pores was observed in micron size and interconnected, which make it as desirable characteristic to achieve a good penetration of the dyes and electrolyte particles throughout the pore structure of **TO**. These pores are the main microstructural feature of the high specific surface area **TO** nanoparticle coating. The nanoparticles structure is useful because it has a high effective surface area which the molecules of the dyes extracts can be linked (Hayles, 2014).

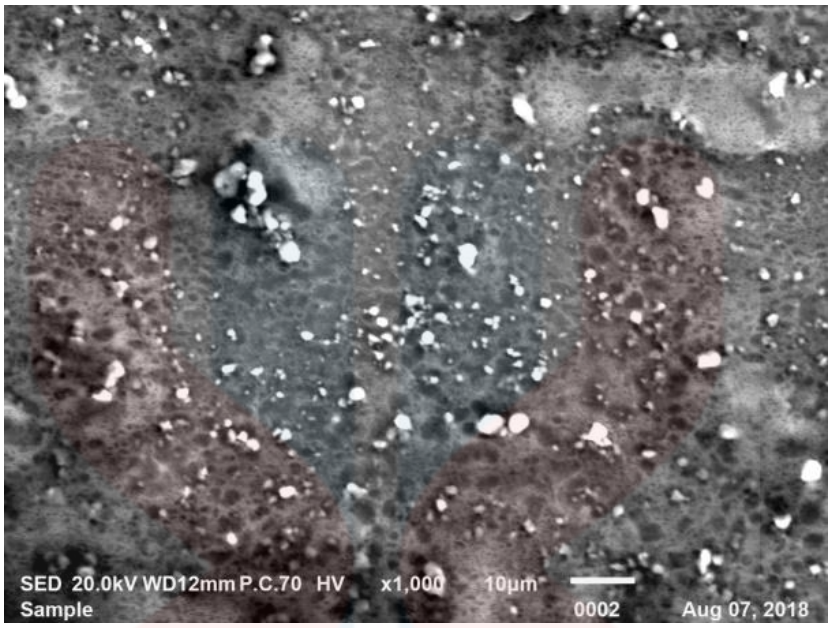

Figure 4.9: The morphology of **TO**/**DF**/ITO glass.

Figure 4.10 provides SEM morphology of **AO**/**DF**/ITO image of the results at the magnification of 300 x. From Figure 4.10, it can be seen that, the **AO** thin films shows the relatively porous surface morphology. The SEM image of **AO** template film shows the diameter of pore is 50 µm. The presences of **DF** dyes on the **AO** make the surface of **AO** film has pores in micron size and are interconnected to each other. The image form on **AO**/**DF**/ITO films have no clear grain structure, suggesting that they are amorphorous, the as-deposited ITO film on the **AO** layer exhibits a clear grain structure, suggesting that it is crystalline. (Woo *et al*., 2011).

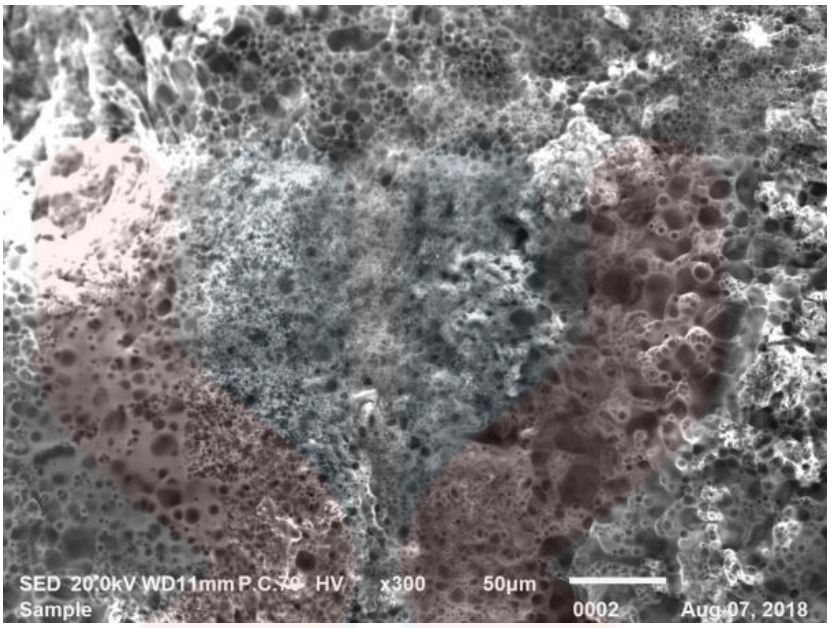

Figure 4.10: The morphology of **AO**/**DF**/ITO glass.

Figure 4.11 provides SEM morphology of **ZO**/**DF**/ITO image of the results at the magnification of 1000 x. **ZO** is typically appeared in a random rough porous structure formation. The average diameter of these **ZO** particles was around 50 µm. It is clear that **ZO** particle exhibit as granular structure composed of small grains with light and dark color that appear somehow aggregated with porosity around. **AO**/**DF**/ITO sample has smooth structure on the background with small granular structure. As known, **AO** have several pores with many inner surfaces, which can be definitely permeated with the matrix. Thus, the surface of **AO**/**DF**/ITO sample has smooth background structures for the reason that the supporting materials diffuse well in matrix (Genc *et al*., 2015).

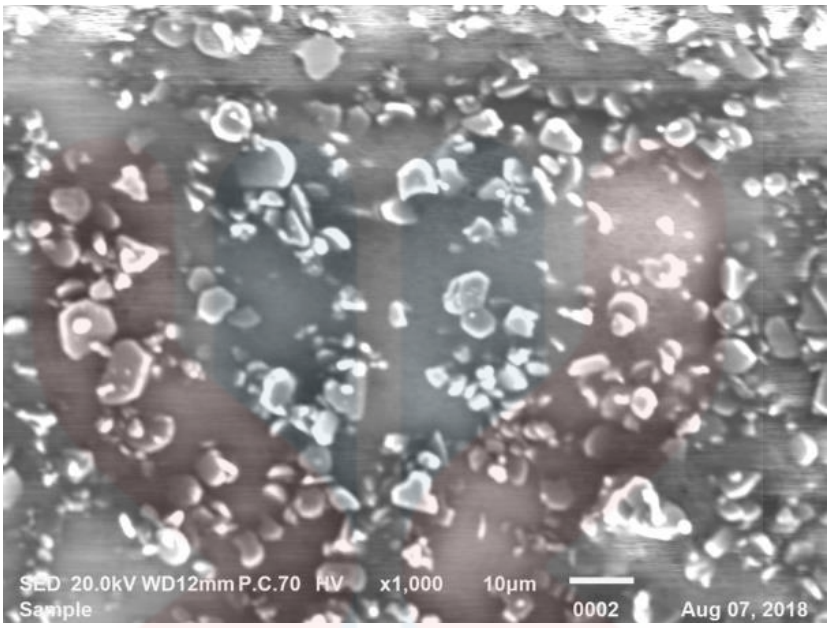

Figure 4.11: The morphology of **ZO**/**DF**/ITO glass.

4.5 The Conductivity Measurement

Four-point probe (4PP) was used to measure the resistivity as well as the voltage flow of the conductive samples. 4pp is used in this study to determine the conductivity of the surface layer in dyes-sensitized solar cell (DSSC). This measurement was used to measure sheet resistance, Rs by employing set of equations which the value of the electrical conductivity can be calculated (Bautista, 2004). Table 4.2 shows the summaries of conductivity results.

Table 4.2: The conductivity values of **DF**/ITO and **MO**/**DF**/ITO (**MO** = **TO**, **AO** and **ZO**).

	Light (200 W/M^2)	
	R_S = 4.532 x V/I (Ωm)	**σ = 1/R_S (Scm^{-1})**
DF/ITO	26.6935	3.75E-04
TO/**DF**/ITO	13.7773	7.26E-04
AO/**DF**/ITO	23.3851	4.28E-04
ZO/**DF**/ITO	18.5812	5.38E-04

From the result obtained, **DF**/ITO, **TO**/**DF**/ITO, **AO**/**DF**/ITO and **ZO**/**DF**/ITO the sheet resistance has the result the value of 26.6935, 13.7773, 23.385 and 18.5812 Ωm respectively. While the result summarized of **DF**/ITO, **TO**/**DF**/ITO, **AO**/**DF**/ITO and **ZO**/**DF**/ITO for the conductivity value of 3.75×10^{-4}, 7.26×10^{-4}, 4.28×10^{-4} and 5.38×10^{-4} Scm^{-1} respectively. Clearly, the DSSC with nanoparticle sizes of **TO** have higher conductivity than those with large particle size of **ZO** and **AO**. The lower conductivity in large particle sizes of **AO** and **ZO** layer can be qualified to a strong back-scattering light and can consequence in lower conductivity result.

From this study, it is identified that the smaller particle size of **TO** layer has the large surface area compared to the large one. The number of absorbed dyes in small particle size of **TO** layer is greater than in the large particle size of **ZO** and **AO** layer due to the large surface area. Hence, the smaller the surface area of particles, the higher the conductivity results.

4.6 Solar Cell Measurement

Solar cell measuremnet was conducted by using the Electrochemical Impedence Spectroscopy (EIS) (Metrohm Autolab). EIS is functional to measure the solar cell performance of dye-sensitized solar cells (DSSC). One of the most important measurements of a solar cell is the current - voltage (IV) measurement. The intensity of the illumination is standardized to 1000 W/m^2, equal to 1 sun. The IV physical characteristics are observed under illumination by smearing an external potential between the working and counter electrode. The external potential is altered from I_{sc} to V_{oc} or opposite depending on scanning direction. The IV measurements would be carried out with sufficient slow scan rate so the solar cell has time to adjust and no hysteresis effects appear. The supreme power point is given by the P_{max} values. By this the fill factor (FF) is calculate as the a measure of the ratio of the P_{max} and V_{oc} .

According to Table 4.3, it showed that **TO**/**DF**/ITO has the highest power conversion efficiency (PCE) with 5.20 % followed by **ZO**/**DF**/ITO, **AO**/**DF**/ITO and **DF**/ITO with 4.35 %, 3.32 % and 1.58 % respectively.

Table 4.3: The values obtained from solar cell measurement.

	Voc	**Isc**	**Pmax**	**PCE (%)**	**FF**
DF/ITO	1.92E-01	2.08E-04	6.32E-07	1.58	1.77E-01
TO/DF /ITO	1.02E-01	2.66E-05	1.62E-06	5.20	2.85E-01
AO/DF /ITO	1.84E-01	2.29E-05	1.33E-06	3.32	2.46E-01
ZO/DF /ITO	1.15E-01	2.51E-05	1.74E-06	4.35	2.65E-01

Table 4.3 summarizes the efficiency, fill factor, open circuit voltage and short circuit currentfor the corresponding of solar cells efficiency trend of **DF**/ITO, **TO**/**DF**/ITO, **AO**/**DF**/ITO and **ZO**/**DF**/ITO respectively. DSSC with the **TO**/**DF**/ITO film exhibited the highest light-to-electric energy conversion efficiency of 5.20 % comparable with conducting of **TO**/dye/ITO reported in the literature (Hossain *et al*., 2017) **TO**/**DF**/ITO gave the highest efficiency, despite the lowest absorbance value. Compared to **ZO**/**DF**/ITO and **AO**/**DF**/ITO with conversion efficiency of 3.32 % and 4.35 % respectively. This is might be the analysis of the chemical properties of the dye and electrons reactions between the dye and **TO**. Higher efficiencies will accredited to the rich of absorption of dye molecules onto the **TO** particles (Desilvestro *et al*., 1985). A nanoparticle of **TO** will provided a paths for the electrons while maintaining a low surface area for the dye absorption. Hence, the accessibility of bonds between dye and **TO** molecules through which electrons can transport from the excited dye molecules to the **TO** film has been stated to result in high efficiencies (Nwanya *et al*., 2012). In DSSCs with nanoparticle size of **TO** exhibit the highest PCE than those with larger particle sizes of **ZO** and **AO**. It earnings that the interface between layers with different particle sizes will be an significant factor to disturb the solar performance except for the allowing for back-scattering light and surface area.

The power conversion efficiency for **DF**/ITO was 1.58 % which the lowest efficiencies compared to the **MO**/**DF**/ITO. This is because, the wide band gap of **MO** having a appropriate band position relative to sensitizer has been working for the fabrication of DSSC. On the other hand, dye is only accountable for the absorption of the light at visible and near-infrared region. The strong absorption of light is qualified to the

intramolecular charge transfer transition (ICT) commencing electron donating group to the anchoring acceptor group of dye. Therefore, the anchored dye on the **MO** surface supports the red shift of absorption threshold of **MO** near infrared region (Rengaraj *et al*., 2006). Hence, from the analysis we can conclude that, DSSC coated with **TO** has highest conversion efficiencies after tuning the bandgap.

CHAPTER 5

CONCLUSION AND RECOMMENDATION

5.1 Conclusion

In this study, the preparation of *Hylocereus polyrhizus sp*. (dragon fruit) dye extracts were successfully extracted and prepared. These dye extracts were characterized by using UV-Vis and SEM. The dye extracts solution was analyzed using UV-Vis in order to evaluate the solar absorption at the wavelength region from 400 nm to 800 nm. The results of absorption spectra showed that the absorbance peak reading is 446 nm. The bandgap value of **DF** solution was determined from the Tauc plot with value of 2.15 eV.

The bandgap value was determined from the Tauc plot. From the results, it showed that there are different value in bandgap energy, where the value of each sample **TO**/ITO

followed by **ZO**/ITO and **AO**/ITO with 2.75 eV, 3.65 eV, and 2.96 eV respectively. Compared to the **MO**/**DF**/ITO the **TO**/**DF**/ITO also has the lowest value of bandgap energy which is 1.55 eV follwed by **ZO**/**DF**/ITO and **AO**/**DF**/ITO which are 2.60 eV and 2.80 eV respectively the **TO**/**DF**/ITO also has the lowest value of bandgap energy which is 1.55 eV follwed by **ZO**/**DF**/ITO and **AO**/**DF**/ITO which are 2.60 eV and 2.80 eV respectively.

The surface morphology from sample **DF**/ITO. **TO**/**DF**/ITO, **AO**/**DF**/ITO and **ZO**/**DF**/ITO showed a different image. The morphology of **DF** on ITO glass formed clusters of small holes structure with large surface area by having average size of 100 µm using 200 x of magnification. The morphology of **TO**/**DF**/ITO with the magnification of 1000 x and the size of porous are 10 µm that there was no agglomerations of particles and the particle distribution is uneven and white particles on the image are **TO** nanoparticles. Next, SEM morphology of **AO**/**DF**/ITO image of the results at the magnification of 300 x can be seen that, the **AO** thin films shows the relatively porous surface morphology and template film shows the diameter of pore is 50 µm. while, SEM morphology of **ZO**/**DF**/ITO image of the results at the magnification of 1000 x show that the average diameter of these **ZO** particles was around 50 µm. It is clear that **ZO** particle exhibit as granular structure composed of small grains with light and dark color that appear somehow aggregated with porosity around. Last but not least,

Four-point probe (4PP) was used to measure the resistivity and conductivity of devices. From the result obtained, **DF**/ITO, **TO**/**DF**/ITO, **AO**/**DF**/ITO and **ZO**/**DF**/ITO the sheet resistance has the result the value of 26.69, 13.78, 23.39 and 18.58 Ωm respectively. In addition, the conductivity value for **DF**/ITO, **TO**/**DF**/ITO, **AO**/**DF**/ITO and **ZO**/**DF**/ITO were 3.75×10^{-4}, 7.26×10^{-4}, 4.28×10^{-4} and 5.38×10^{-4} Scm^{-1} respectively.

The results of solar cell obtained from electrochemical impedance spectroscopy (EIS) for each metal oxide showed where **TO**/**DF**/ITO has the highest power conversion efficiency (PCE) recorded with 5.20 % followed by **ZO**/**DF**/ITO, **AO**/**DF**/ITO and **DF**/ITO with 4.35 %, 3.32 % and 1.58 % respectively.

Therefore, from the overall results, suggesting that the highest PCE of TO/DF/ITO is the best sample to be used as dye-sensitized solar cell (DSSCs) due to the absorbance range of 400 nm to 600 nm, lowest bandgap value of 1.55 eV and SEM morphology formed was clusters of small holes structure with large surface area by having average size of 100 µm using 200 x of magnification.

5.2 Recommendation

In a DSSC, many factors can influence the overall conversion efficiency. In this thesis, we have focussed on the different metal oxide with dye extract in performance of DSSC. As the titanium dioxide paste was applied by Dr Blading method, the resulting thickness was a delicate function of the applied pressure, which was controlled manually. To obtain better reproducibility, a screen printing technique may be introduced. For optimization of the titanium dioxide structure, a measurement strategy for surface roughness, effective surface area and film porosity is needed to be introduced. SEM data only gave a raw insight to these parameters.

To obtain a better layer of photoanode is by improving the methodologies in dissolving of metal oxide. Metal oxide can usually dissolved in strong mineral acids or

reductants. The chemistry of metal oxide complexes in low-temperature ionic liquids has received little attention. Thus, from previous study, the metal oxide was found to be very soluble in mineral acids.

A sputtered platinum electrode may be introduced, to improve charge collection as well as light absorption by reflecting the unabsorbed light back with a mirror action. Some less important enhancements like - soldered contact, anti-reflective coating and low sheet resistance substrates may also be introduced.

The comfort of fabrication and price effectiveness of DSSC makes it practicable and effective solar cells for the future. It is predictable that the low cost for commercially fabricating DSSCs alongside with its respectable performance will absolutely substitute conservative solar cells very preferably. Researches are working on for improving the efficiency and capability of the cell. DSSCs are immobile at the start of their improvement cycle. Efficiency additions are imaginable and have newly started more widespread study. These consist of the use of efficient photo sensitizers for conversion of higher-energy light into numerous electrons, using solid-state electrolytes for well temperature response, and fluctuating the doping of the TiO_2 to improved match it with the electrolyte being used. Finally, even though there have been a numeral of initial studies into the improvement of DSSC modules, a comprehensive understanding of generally efficiencies, life times and degradation mechanisms of fresh efficient stable DSSC module.

REFERENCES

Abdel-Latif, M. S., Batniji, A., El-Agez, T. M., Younis, M. J., Ghamri, H., Thaher, B. A. A., … Taya, S. A. (2016). Dye sensitized solar cells based on hydrazonoyl synthetic dyes. *Journal of Nano- and Electronic Physics*, *8*(4).

Ahmad, R., Ali, M., & Nayan, N. (2010). Fabrication and analysis of dye-sensitized solar cell using natural dye extracted from dragon fruit. *International Journal of Integrated Engineering*, *2*(3), 55–62.

Ayalew, W. A., & Ayele, D. W. (2016). Dye-sensitized solar cells using natural dye as light-harvesting materials extracted from Acanthus sennii chiovenda flower and Euphorbia cotinifolia leaf. *Journal of Science: Advanced Materials and Devices*, *1*(4), 488–494.

Bautista, K. (2004). Four-Point Probe Operation Four-Point Probe Operation. *Film*, 1–8.

Bella, F., Gerbaldi, C., Barolo, C., & Grätzel, M. (2015). Aqueous dye-sensitized solar cells. *Chemical Society Reviews*, *44*(11), 3431–3473.

Calogero, G., Di Marco, G., Cazzanti, S., Caramori, S., Argazzi, R., Di Carlo, A., & Bignozzi, C. A. (2010). Efficient dye-sensitized solar cells using red turnip and purple wild Sicilian prickly pear fruits. *International Journal of Molecular Sciences*, *11*(1), 254–267.

Chang, H., & Lo, Y. J. (2010). Pomegranate leaves and mulberry fruit as natural sensitizers for dye-sensitized solar cells. *Solar Energy*.

Desilvestro, J., Grätzel, M., Kavan, L., Moser, J., & Augustynski, J. (1985). Highly Efficient Sensitization of Titanium Dioxide. *Journal of the American Chemical Society*, *107*(10), 2988–2990.

Fang, W., Xing, M., & Zhang, J. (2017). Modifications on reduced titanium dioxide photocatalysts: A review. *Journal of Photochemistry and Photobiology C: Photochemistry Reviews*, *32*, 21–39.

Fujishima, A., Zhang, X., & Tryk, D. A. (2007). Heterogeneous photocatalysis: From water photolysis to applications in environmental cleanup. *International Journal of Hydrogen Energy*, *32*(14), 2664–2672. https://doi.org/10.1016/j.ijhydene.2006.09.009

Genc, Z. K., Canbay, C. A., Acar, S. S., Sekerci, M., & Genc, M. (2015). Preparation and thermal properties of heterogeneous composite phase change materials based on camphene-palmitic acid. *Journal of Thermal Analysis and Calorimetry*, *120*(3), 1679–1688.

Gómez-Ortíz, N. M., Vázquez-Maldonado, A., Pérez-Espadas, Mena-RejónG. J., Azamar-Barrios, J. A., & Oskam, G. (2010). Dye-sensitized solar cells with natural dyes extracted from achiote seeds. *Solar Energy Materials and Solar Cells*, *94*(1), 40–44.

Goncalves, L. M., De Zea Bermudez, V., Ribeiro, H. A., & Mendes, A. M. (2008). Dye-sensitized solar cells: A safe bet for the future. *Energy and Environmental Science*, *1*(6), 655–667.

Graetzel, M. (2009). Recent Advances in Sensitized Mesoscopic Solar Cells. *Accounts of Chemical Research*, *42*(11), 1788–1798. h

Harris, N. N., Javellana, J., Davies, K. M., Lewis, D. H., Jameson, P. E., Deroles, S. C., Schwinn, K. E. (2012). Betalain production is possible in anthocyanin-producing plant species given the presence of DOPA-dioxygenase and L-DOPA. *BMC Plant Biology*, *12*(March).

Hayle, S. T. (2014). Synthesis and Characterization of Titanium Oxide Nanomaterials Using Sol-Gel Method. *American Journal of Nanoscience and Nanotechnology*, *2*(1), 1.

Herbach, K. M., Rohe, M., Stintzing, F. C., & Carle, R. (2006). Structural and chromatic stability of purple pitaya (Hylocereus polyrhizus [Weber] Britton & Rose) betacyanins as affected by the juice matrix and selected additives. *Food Research International*, *39*(6), 667–677.

Hernandez-Martinez, A. R., Estevez, M., Vargas, S., Quintanilla, F., & Rodriguez, R. (2011). New dye-sensitized solar cells obtained from extracted bracts of bougainvillea glabra and spectabilis betalain pigments by different purification processes. *International Journal of Molecular Sciences*, *12*(9), 5565–5576.

Hossain, M. K., Pervez, M. F., Mia, M. N. H., Mortuza, A. A., Rahaman, M. S., Karim, M. R., … Khan, M. A. (2017). Effect of dye extracting solvents and sensitization time on photovoltaic performance of natural dye sensitized solar cells. *Results in Physics*, *7*, 1516–1523.

Isah Kimpa, M., Momoh, M., Uthman Isah, K., Nawawi Yahya, H., & Muhammed Ndamitso, M. (2012). Photoelectric Characterization of Dye Sensitized Solar Cells Using Natural Dye from Pawpaw Leaf and Flame Tree Flower as Sensitizers. *Materials Sciences and Applications*, *03*(05), 281–286.

Jonathan, E., Onimisi, M., Eli, D., Abdu, S., & Abdulsalam, M. (2016). Photovoltaic Perfomance of Dye Sensitized Solar Cells Using Natural Dyes Extracted from Bougainvillea Flower and Mango Leaves. *Journal of Scientific Research and Reports*, *10*(6), 1–5.

Kantesaria, S. (n.d.). (2014) Optimization of Dye-Sensitized Solar Cells (DSSCs) Through Co-adsorption and Tri-adsorption of Organic Dyes, 1–5.

Kay, A., & Grätzel, M. (1996). Low cost photovoltaic modules based on dye sensitized nanocrystalline titanium dioxide and carbon powder. *Solar Energy Materials and Solar Cells*, *44*(1), 99–117.

Kazici, M., Bozar, S., Gürşen, A., Ongül, F., Karsli, A., Sariciftci, N. S., & Günes, S. (2018). Solar Cells. Comprehensive Energy Systems, 4–5(7), 637–658.

Kazmi, S. A., Hameed, S., & Azam, A. (2016). Synthesis and characterization of Ag nanowires: Improved performance in dye sensitized solar cells. *Perspectives in Science*, *8*, 577–579.

Klassen, S. (2011). The Photoelectric Effect: Reconstructing the Story for the Physics Classroom. *Science and Education*, *20*(7), 719–731.

Krebs, F. C., Hösel, M., Corazza, M., Roth, B., Madsen, M. V., Gevorgyan, S. A., Jørgensen, M. (2013). Freely available OPV—The fast way to progress. *Energy Technology*, *1*(7), 378–381.

Kumara, N. T. R. N., Ekanayake, P., Lim, A., Liew, L. Y. C., Iskandar, M., Ming, L. C., & Senadeera, G. K. R. (2013). Layered co-sensitization for enhancement of conversion efficiency of natural dye sensitized solar cells. *Journal of Alloys and Compounds*, *581*, 186–191.

Maldonado-Valdivia, A. I., Galindo, E. G., Ariza, M. J., & García-Salinas, M. J. (2013). Surfactant influence in the performance of titanium dioxide photoelectrodes for dye-sensitized solar cells. *Solar Energy*, *91*, 263–272.

Mazhdi, M., Torkzadeh, F., & Mazhdi, F. (2013). International Journal of Bio-Inorganic Hybrid Nanomaterials Optical , Photoluminescence and Thermoluminescence Properties Investigation of ZnO and Mn Doped ZnO Nanocrystals, (4), 233–241.

Mohammad Bagher, A. (2015). Types of Solar Cells and Application. *American Journal of Optics and Photonics*, *3*(5), 94.

Mok, T. M., & O'Leary, S. K. (2007). The dependence of the Tauc and Cody optical gaps associated with hydrogenated amorphous silicon on the film thickness: αl Experimental limitations and the impact of curvature in the Tauc and Cody plots. *Journal of Applied Physics*, *102*(11).

Nivea, R., Gunasekaran, V., Kannan, R., Sakthivel, T., & Govindan, K. (2014). Enhanced photocatalytic efficacy of hetropolyacid pillared TiO_2 nanocomposites. *Journal of Nanoscience and Nanotechnology*, *14*(6), 4383–4386.

Nocera, D. G., & Nash, M. P. (2007). For the '"In This Issue'''' summary,"' *104*(42).

Nwanya, A. C., Ugwuoke, P. E., Ejikeme, P. M., Oparaku, O. U., & Ezema, F. I. (2012). Jathropha curcas and citrus aurantium leaves dye extract for use in dye sensitized solar cell with TiO_2 films. *International Journal of Electrochemical Science*, *7*(11), 11219–11235.

Oprea, C. I., Panait, P., Cimpoesu, F., Ferbinteanu, M., & Gîrţu, M. A. (2013). Density functional theory (DFT) study of coumarin-based dyes adsorbed on TiO2nanoclusters-applications to dye-sensitized solar cells. *Materials*, *6*(6), 2372–2392.

Oviri, O. K., & Ekpunobi, A. J. (2013). Transmittance and Band Gap Analysis of Dye Sensitized Solar Cell, *2*(1), 25–31.

Priyantha, N., Lim, L. B. L., & Dahri, M. K. (2015). Dragon fruit skin as a potential biosorbent for the removal of methylene blue dye from aqueous solution. *International Food Research Journal*, *22*(5), 2141–2148.

Rengaraj, S., Li, X. Z., Tanner, P. A., Pan, Z. F., & Pang, G. K. H. (2006). Photocatalytic degradation of methylparathion - An endocrine disruptor by Bi3+-doped TiO2. *Journal of Molecular Catalysis A: Chemical*, *247*(1–2), 36–43.

Shanmuga Priya, S., Rao, A., Thirunavukkarasu, I., & Nayak, V. (2016). Solar pebble bed reactor for treatment of textile and petrochemical industrial wastewater. *International Journal of ChemTech Research*, *9*(11), 261–270.

Simiao, S., & Wilms, S. (2015). Venerating the root : Sun SiMiao's Essential prescriptions worth a thousand in gold for every emergency. Pediatrics. Part two., *13*(1), 544.

Stintzing, F. C., & Carle, R. (2004). Functional properties of anthocyanins and betalains in plants, food, and in human nutrition. *Trends in Food Science and Technology*, *15*(1), 19–38.

Syafinar, R., Gomesh, N., Irwanto, M., Fareq, M., & Irwan, Y. M. (2015). *Chlorophyll Pigments as Nature Based Dye for Dye-Sensitized Solar Cell (DSSC). Energy Procedia* (Vol. 79). Elsevier B.V.

Tahir, D., Satriani, W., Gareso, P. L., & Abdullah, B. (2018). Dye sensitized solar cell (DSSC) with natural dyes extracted from Jatropha leaves and purple Chrysanthemum flowers as sensitizer. *Journal of Physics: Conference Series*, *979*(1).

Viezbicke, B. D., Patel, S., Davis, B. E., & Birnie, D. P. (2015). Evaluation of the Tauc method for optical absorption edge determination: ZnO thin films as a model system. *Physica Status Solidi (B) Basic Research*, *252*(8), 1700–1710.

Willner, A. E., Byer, R. L., Chang-Hasnain, C. J., Forrest, S. R., Kressel, H., Kogelnik, H., Zervas, M. N. (2012). Optics and photonics: Key enabling technologies. *Proceedings of the IEEE*, *100*(SPL CONTENT), 1604–1643.

Wongcharee, K., Meeyoo, V., & Chavadej, S. (2007). Dye-sensitized solar cell using natural dyes extracted from rosella and blue pea flowers. *Solar Energy Materials and Solar Cells*, *91*(7), 566–571.

Woo, K. K., Ngou, F. H., Ngo, L. S., Soong, W. K., & Tang, P. Y. (2011). Stability of Dragon Fruit. *American Journal of Food Technology*.

APPENDIX

Figure A, 1: Electrochemical impendence spectra (EIS) of **DF**/ITO

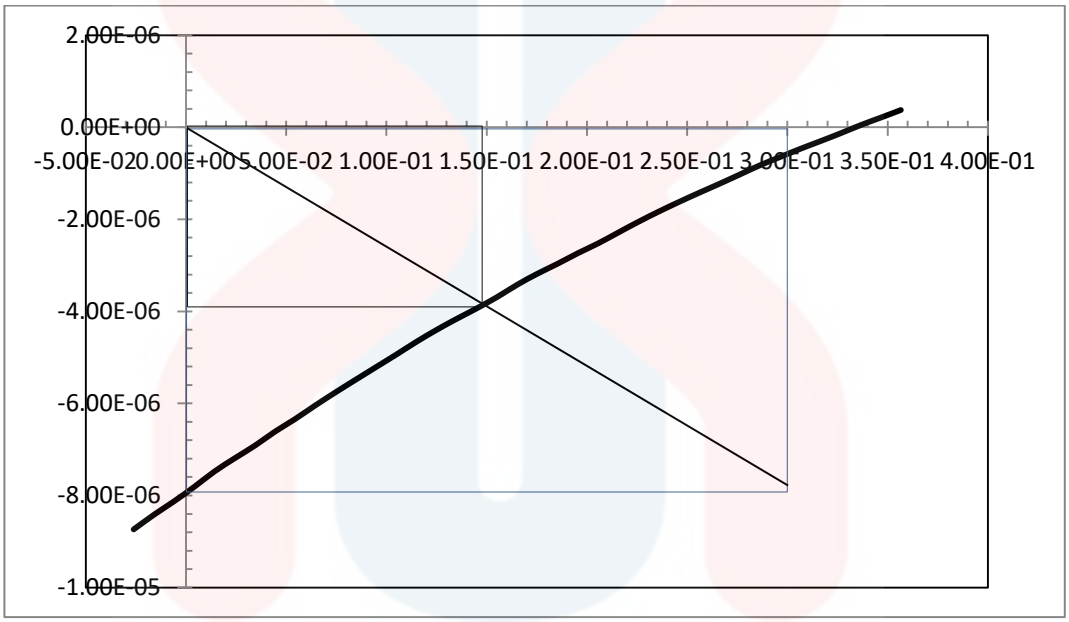

Voc	1.92E-01
Isc	2.08E-04
Pin	4.00E-05
Pmax	6.32E-07
FF	1.77E-01
PCE	1.58

Figure A, 2: Electrochemical impendence spectra (EIS) of **TO**/**DF**/ITO

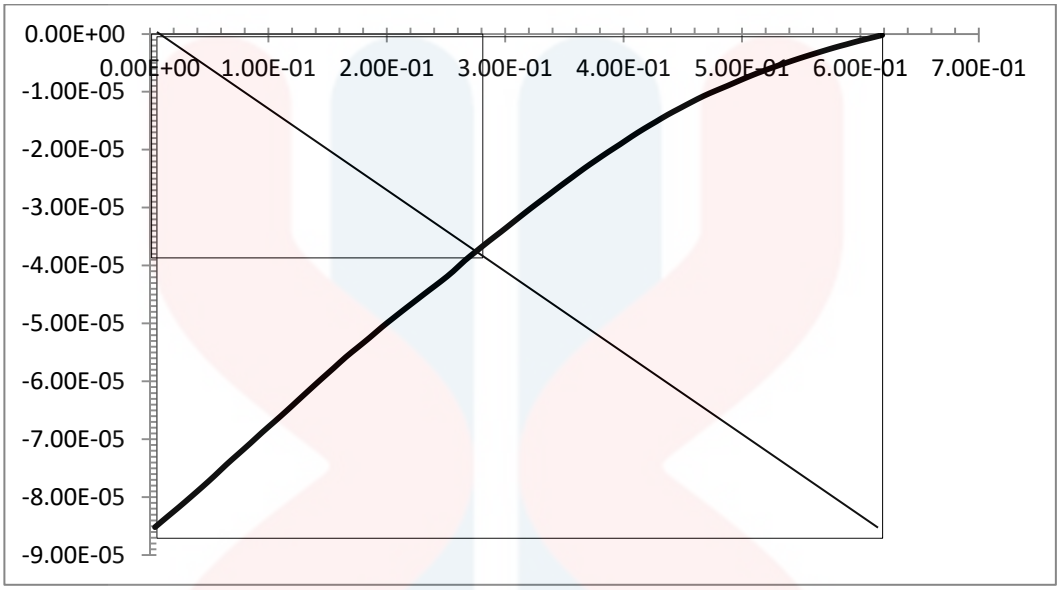

Voc	1.02E-01
Isc	2.66E-05
Pin	4.00E-05
Pmax	1.62E-06
FF	2.85E-01
PCE	5.20

Figure A, 3: Electrochemical impendence spectra (EIS) of **AO**/**DF**/ITO

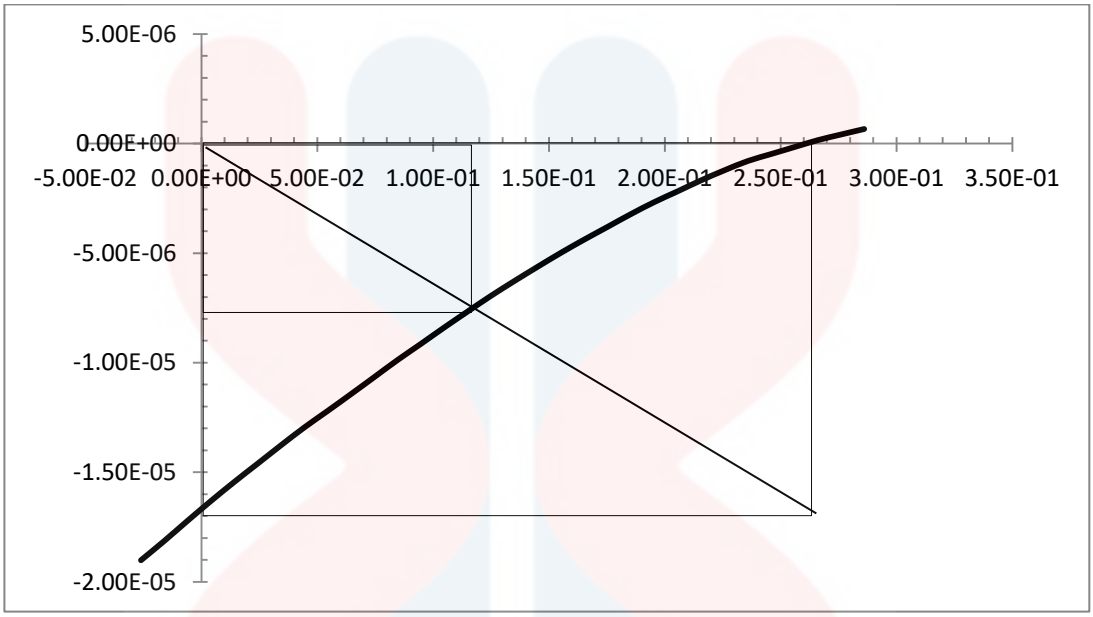

Voc	1.84E-01
Isc	2.51E-05
Pin	4.00E-05
Pmax	1.33E-06
FF	2.46E-01
EFF	3.32

Figure A, 4: Electrochemical impendence spectra (EIS) of **ZO**/**DF**/ITO

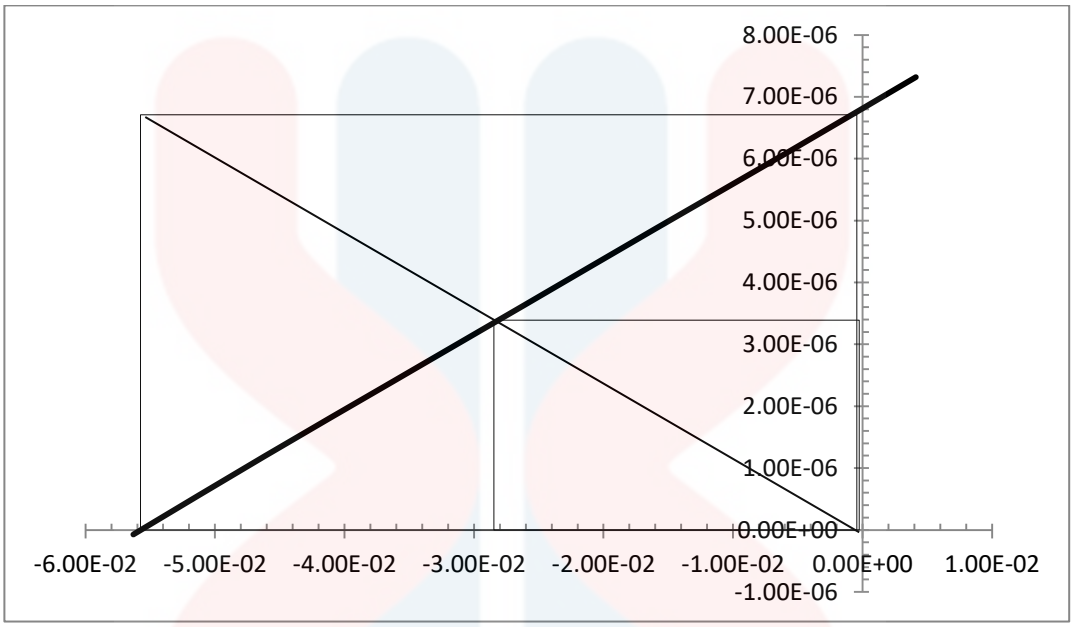

Voc	1.15E-01
Isc	2.51E-05
Pin	4.00E-05
Pmax	1.74E-06
FF	2.65E-01
PCE	4.35